NACA TN 3490

NATIONAL ADVISORY COMMITTEE FOR AERONAUTICS

TECHNICAL NOTE 3490

EXPERIMENTAL AND CALCULATED TEMPERATURE AND MASS HISTORIES OF VAPORIZING FUEL DROPS

By M. M. El Wakil, R. J. Priem, H. J. Brikowski,
P. S. Myers, and O. A. Uyehara

University of Wisconsin

Washington

January 1956

NATIONAL ADVISORY COMMITTEE FOR AERONAUTICS

TECHNICAL NOTE 3490

EXPERIMENTAL AND CALCULATED TEMPERATURE AND MASS HISTORIES OF VAPORIZING FUEL DROPS

By M. M. El Wakil, R. J. Priem, H. J. Brikowski, P. S. Myers, and O. A. Uyehara

SUMMARY

The present report compares experimental and calculated mass and temperature histories of drops vaporizing with a constant velocity relative to the air and confirms the thought that, under many conditions, the unsteady state or time required for the drop to reach the wet-bulb temperature is an appreciable portion of the total vaporization time.

Work was done to verify or disprove the assumptions used in the computations. Data are presented to show that the assumption of infinite thermal conductivity is valid primarily because of circulation inside the drop. The presence of this circulation was verified by high-speed motion pictures. The need for a correction factor to the heat transfer to express the effect of mass transfer on heat transfer was confirmed as well as the need for a correction factor to correct for unidirectional (as opposed to equimolal) diffusion.

Work was also done to evaluate the extent and effect of heat transfer down the thermocouple wires supporting the drop. It was shown that if wires of large diameter or high thermal conductivity were used the heat transfer was not negligible. The experimental data were then taken using small-diameter wires of low thermal conductivity.

Calculations were also performed using different heat-transfer correlations as well as different types of averaging the properties of the film. It was found that the biggest variation was in the value of the diffusion coefficient. By using the highest computed value for the diffusion coefficient, the use of the correlations of Ranz and Marshall in the computations produced curves that agreed reasonably well with the experimental curves.

A few preliminary temperature histories of the vaporizing drops of binary mixtures were also taken as well as a few histories of drops of different fuels vaporizing in air at sufficiently high temperatures that burning of the drops took place. While precise temperature histories were not obtained the measured steady-state temperatures were close to the boiling temperatures when burning occurred.

INTRODUCTION

Fuel injected into a combustion chamber by a nozzle leaves the nozzle orifice as sheets or ligaments which eventually break down into drops of varying sizes. As soon as these drops are formed, they start heating up to their steady-state or wet-bulb temperatures, which are a function of the type of fuel used and the temperature and pressure of the surrounding air.

The importance of the fraction of the total vaporization time of a fuel drop occupied by the unsteady-state or heating-up portion was stressed in a previous theoretical investigation (ref. 1). It was estimated from calculated data that the larger drops emanating from a jet-engine combustion-chamber injector reach the combustion zone while still in the unsteady state. Consequently, it is believed that computations which include only the wet-bulb or steady-state portion of the vaporization time of fuel drops do not present a true picture of the time elapsed and the distance traveled before combustion occurs in the heterogeneous mixture that exists in a jet-engine combustion chamber.

Reasonable agreement between experiment and theory was reached and progress was made in understanding the effects of many variables entering into the calculation. It is believed that if the equations can be verified for use on small drops they will be of help in understanding the complex phenomena that occur prior to the combustion zone of a jet-engine combustion chamber.

This investigation was conducted at the University of Wisconsin under the sponsorship and with the financial assistance of the National Advisory Committee for Aeronautics.

SYMBOLS

A	area, sq in.
A_o	surface area of liquid drop, sq in.
B_o	thickness of air-vapor film surrounding drop, in.
C_1, C_2...	constants
c_{pf}	specific heat of fuel vapor at constant pressure, Btu/(lb)(°F)
c_{pL}	specific heat of liquid fuel, Btu/(lb)(°F)

c_{pm} specific heat of air-vapor mixture, Btu/(lb)(°F)

D_v diffusion coefficient of air-vapor system, sq in./sec

d_v diffusion velocity with respect to a plane moving at mass average velocity, in./sec

E_L internal energy of liquid, Btu/lb

F mass flux vector for vapor with respect to liquid surface, lb/(sq in.)(sec)

f molal mass flux vector for vapor with respect to liquid surface, lb mole/(sq in.)(sec)

H molecular enthalpy, Btu/lb

$H_L = E_L + pV_L$

h coefficient of heat transfer, Btu/(sq in.)(sec)(°F)

I heat flux with respect to liquid surface, Btu/(sq in.)(sec)

J_i mass flux vector of component i with respect to a plane moving at mass average velocity, lb/(sq in.)(sec)

K thermal conductivity, Btu/(in.)(sec)(°F)

K_g coefficient of mass transfer, 1/sec

K_m average thermal conductivity in air-vapor mixture, Btu/(in.)(sec)(°F)

L energy transported to liquid surface, Btu/sec

M molecular weight, lb/mole

M_a molecular weight of air, lb/mole

M_f molecular weight of fuel, lb/mole

M_L mass of liquid drop, lb

M_m apparent molecular weight of air-vapor mixture, lb/mole

m	total mass vaporized from drop, lb
m_i	mass of molecule of component i, lb/molecule
m_L	molecular mass of liquid, lb/molecule
N_{Nu}	Nusselt number for heat transfer, unitless
N_{Nu}'	Nusselt number for mass transfer, unitless
N_{Re}	Reynolds number, unitless
N_{Sc}	Schmidt number, unitless
n	total number density, $\sum n_i$
n_i	number density of any component i, molecules/cu in.
n_L	number density of liquid, molecules/cu in.
P_T	total pressure, lb/sq in.
p	partial pressure, lb/sq in.
p_a	partial pressure of air, lb/sq in.
p_f	partial pressure of fuel vapor, lb/sq in.
p_{fb}	partial pressure of fuel vapor at film boundary considered to be zero, lb/sq in.
p_{fL}	partial pressure of fuel vapor at liquid surface, equal to liquid vapor pressure, lb/sq in.
Q	total heat transfer from air to drop, Btu/sec
Q_L	sensible heat received by drop, Btu/sec
Q_o	heat arriving at inner segment inside drop, Btu/sec
Q_s	heat carried back with diffusing vapor in form of superheat, Btu/sec

Q_v heat received at drop surface, Btu/sec

q energy flux vector with respect to a plane moving at mass average velocity, Btu/(sq in.)(sec)(^oF)

R universal gas constant, in-lb/(mole)(^oF)

r radius at any point in film, in.

r_f molal rate of diffusion of fuel vapor at radius r in film, moles/(sq in.)(sec)

r_{fo} molal rate of diffusion of fuel vapor at liquid surface, moles/(sq in.)(sec)

r_o radius of drop or increment of drop, in.

T temperature in film at radius r, ^oR

T_{as} asymptotic or wet-bulb temperature of drop, ^oR

T_B air temperature at film boundary, ^oR

T_L temperature of liquid drop, ^oR

T_m mean temperature in film or segment of drop, ^oR

V_d velocity of one component with respect to other in a two-component diffusion system, in./sec

V_L absolute velocity of liquid surface, in./sec

U velocity of drop with respect to air, in./sec

w rate of mass of vapor diffused out, lb/sec

x thickness of segments within drop, in.

Z correction factor for heat transfer, $\frac{z}{e^z - 1}$, unitless

$$z = \frac{wc_{pf}}{4\pi K_m} \frac{B_o}{r_o(r_o + B_o)}$$

α correction factor for mass transfer, unitless

θ time, sec

θ_t total time of vaporization of liquid drop, sec

ρ density, lb/cu in.

ρ_a density of air, lb/cu in.

ρ_L density of liquid drop, lb/cu in.

ρ_m density of air-vapor mixture in film, lb/cu in.

ρ_n mass density of mixture, lb/cu in.

λ latent heat of vaporization, Btu/lb

Subscripts:

i component i

1 component 1 or segment 1

2 component 2 or segment 2

Superscripts:

o condition of extremely small pressure difference

* reduced value

APPARATUS

The experimental apparatus shown schematically in figure 1 was designed to meet two requirements: One, to study a drop of fuel under conditions as close as practicable to the conditions encountered by drops in a combustion chamber, and, two, to obtain accurate temperature and radius histories of the drop.

Temperature histories were obtained by hanging a drop on a thermocouple and recording the output of the thermocouple with a recorder. The output of the thermocouple was recorded when a sudden blast of heated air was passed over the drop. Drops of fuel of 99-percent mole purity were formed on the thermocouple with a syringe and hypodermic needle and their instantaneous radius was recorded by means of a motion-picture camera.

As shown in figure 1, air from a laboratory line at 80 pounds per square inch gage was passed through a porous stone filter and was metered by controlling the pressure on either or both of two critical flow orifices. After metering, the air was electrically heated and then passed into a calming section consisting of a 21-inch length of 4-inch pipe with internal flow control as shown in figure 1. The nozzle at the end of this section was constructed according to the standard specifications for flow nozzles of the International Standards Association and provided a stream of air of known velocity having a comparatively flat velocity profile. A metal deflector prevented the air blast from passing over the drop except when desired. When this deflector was suddenly removed, the drop was subjected to a sudden blast of air. Smoke tests showed that the air formed a smooth cylindrical column for some distance above the thermocouple.

Absolute velocity measurements (using an Illinois Testing Laboratory velometer accurate to about 5 feet per minute) were made at the thermocouple location above the nozzle. The exact velocity profile could not be determined with the velometer, since the velometer nozzle had a 1/4-inch inside diameter. However, no variation in the velometer reading was noticed until the center of the velometer nozzle was 1/8 inch from the outer edge of the 1-inch flow nozzle.

Figure 2 shows a diagram of the circuit used to measure and record the temperature history of the drops. For reasons which will be explained later, 3-mil constantan and manganin wires were used for the thermocouple.

The junctions between the thermocouple wires and the recorder wires were kept in separate ice baths. A switching arrangement, which placed a potentiometer in series with the thermocouple, permitted the zero point of the recorder to be shifted as desired. This arrangement provided good sensitivity irrespective of the temperature level.

The temperature scale for the recorder-thermocouple combination was determined by calibrating the thermocouple in oil. The time scale for the recorder was determined from the known recorder chart speed. It is estimated that, with a chart speed of 26 inches per minute, the error in reading a certain point might be 0.10 second. If the scatter in the experimental wet-bulb temperatures is an indication of the temperature error, then temperatures may be in error by $\pm 4^{\circ}$ F, of which $\pm 2^{\circ}$ F might be scaling error from the recorder chart. The recorder used for the work described above was a modified single-point, strip-chart, 1-second, Speedomax recorder.

It was found that more nearly spherical drops were obtained if either the thermocouple junction was made in the form of a bead or a small bead of some other metal was formed on the junction. Drop shapes during a typical experimental run are shown in figure 3 where the bead and thermocouple leads are shown as shaded areas. The outer line shows the shape of

a drop hanging in zero-velocity air. The second outline shows the shape the drop would take an instant after the air blast is applied. The drop size decreases as vaporization occurs until the surface tension and the force of the air blast move the drop upward on the thermocouple as shown in the figure. The tendency of the drop to blow off or up on the thermocouple determines the maximum permissible air velocity.

Radius histories were obtained by taking a motion picture of an enlarged image of the drop when the image was projected on a ground-glass screen. The optical system and camera are shown schematically in figure 1. A 300-watt projection lamp and reflector served as a light source. The optical system was calibrated by placing a wire of known diameter in place of the drop.

Timing marks were produced on the film by interrupting light from a steady source with a chopper driven by a synchronous motor. The time at which the air-blast deflector was removed was determined by also photographing a neon timing light which was automatically turned on by the removal of the deflector plate. The diameter of the image of the drop on the film was obtained by using a microfilm viewer.

The volume of the drops was determined by assuming that the drop was a sphere having a diameter equal to the largest horizontal diameter measured from the film. This is, of course, not precise, since the drop is somewhat deformed, especially during the initial period. This also does not consider the volume occupied by the thermocouple and its bead; that is, when the liquid had all disappeared one would not state that the drop was 100-percent vaporized. As may be seen in figure 3 the error due to deformation decreases as the drop evaporates. The discrepancy between the surface-volume ratio obtained from exact measurements of the drop size and the ratio obtained by considering the drop as a sphere did not exceed 3 percent.

EXPERIMENTAL RESULTS

Measurement of Surface and Center Temperatures of Drops

The theoretical calculations for the unsteady state presented in reference 1 assumed infinite thermal conductivity within the liquid drop. Both the estimate of the effect of assuming infinite thermal conductivity presented in reference 1 and calculations to be presented later indicated that this assumption might be of questionable validity under certain conditions. Thus an experimental investigation of the temperature gradients, if any, within the drop during the unsteady state were undertaken.

A fuel drop was hung on three equally spaced thermocouples of size-38 manganin-constantan wires as shown in figure 4. The center thermocouple

and one of the two outlying thermocouples were used for temperature measurement while the third was used for symmetry reasons. The outer thermocouple that was used for measurement was connected to the 8 even-numbered points of a 16-point high-speed recorder and the inner thermocouple, to the 8 odd-numbered points. Thus the two thermocouple readings were recorded alternately on the recorder chart.

Cetane was used as the fuel since, because of its low volatility, it would be expected to show a large temperature difference between the center and surface of the drop. Figure 5 shows temperature histories of the center and surface temperatures of a cetane drop. Figure 5 is representative of all cetane drops measured under different air temperatures and velocities. A few experiments were also performed using n-octane as a fuel with similar results. It was concluded from these experimental results that at least over the range of conditions for which data were taken no detectable temperature gradient exists in a drop vaporizing in an air stream.

Internal Circulation in Drops

During the aforementioned studies motion inside the drop was noticed. Since the absence of a temperature gradient in the vaporizing drops could be explained by internal circulation, a photographic study of this movement was undertaken. The result of this photographic study is shown in the film "Circulation in Drops" which is available as a supplement to this Technical Note and can be secured on loan from the Division of Research Information, National Advisory Committee for Aeronautics, Washington, D. C. Such movement has also been observed by other workers (refs. 2 to 5).

For the circulation studies, drops of different fuels were hung on a drawn-glass fiber. A small amount of fine aluminum oxide was mixed with the liquid before forming the drops. The drops were then illuminated and photographed. The motion of the aluminum oxide dust particles within the drops was an indication of internal circulation. It was found that if the dust particles were too fine identification of the particles became difficult because of film grain, while if the dust particles were too coarse they either tended to settle to the bottom of the drop or did not follow the fluid motion.

Motion pictures were taken of drops of n-octane and cetane of approximately 2,000-micron diameter under the following conditions:

(1) n-Octane drops in still air at 70° F with camera speeds of 16, 32, and 64 frames per second

(2) n-Octane drops in an air stream at 250° F with camera speed of 64 frames per second

(3) Cetane drops in still air at 80° F with camera speed of 64 frames per second

(4) Cetane drops in air streams at 250° F with airspeeds of 2, 4, 6, and 8 feet per second and with camera speed of 64 frames per second

(5) A cetane drop in a 6-foot-per-second air stream at 250° F with camera speed of 1,430 frames per second

Frames from these shots are shown in figures 6 and 7. In figure 7 the arrow points to one particular particle. This particle can be seen to change position. The frames shown were seven frames or 1/200 second apart. Figure 8 shows the direction of motion inside the drops with and without an air stream. In all these pictures front illumination was used on the drops. A carbon arc was used for the low-speed pictures (conditions (1) to (4) above), while a zirconium arc was used for the high-speed pictures (condition (5)). A water cell was used to minimize heating of the drops by radiation from the illuminating source.

Heat Transfer From Thermocouple to Drop

The experimentally measured temperature histories of the vaporizing fuel drops were obtained as far as practicable under conditions similar to those encountered by a drop injected into a combustion chamber. Since the drops in the combustion chamber are obviously not hanging from a thermocouple the effect of the supporting device on the heat transfer to the drops is of importance.

Water was used first in the investigation of the effect of the supports because accurate wet-bulb temperatures are available in the literature for a wide range of temperatures. Figure 9 shows three temperature histories of drops of water all vaporizing in a stream of air at 300° F and atmospheric pressure. Curve I was obtained with a 10-mil copper-constantan thermocouple and shows both a high and a continuously rising wet-bulb temperature. Curve II was obtained with a 3-mil copper-constantan thermocouple and shows to a lesser degree the high and continuously rising characteristic of Curve I. Curve III was obtained with a 3-mil manganin-constantan thermocouple and shows an essentially constant wet-bulb temperature. Figure 10 shows the effect of the above three different-size thermocouples on the wet-bulb temperatures of drops of n-octane when subjected to air streams of varying temperatures. The ranges of wet-bulb temperatures shown for the 10- and 3-mil copper-constantan thermocouples represent the total rise of the steady-state temperature reading before the drops evaporated. The range was essentially zero when using a 3-mil manganin-constantan thermocouple.

The above results can be explained on the basis of an appreciable quantity of heat being conducted through the supporting thermocouple wires. If heat is conducted through the thermocouple wires at a constant rate and through the film at a varying rate (because of the decrease in surface area with drop size) a rising wet-bulb temperature curve should result as shown in figure 9. Since manganin has approximately one-fifteenth the thermal conductivity of copper it is believed that the effect of the thermocouple in transferring heat to the drop has been made negligible by a small-size manganin-constantan thermocouple wire as evidenced by curve III of figure 9.

Experimental Temperature and Mass Histories

More than 100 experimental radius and temperature histories have been obtained for the conditions shown in table 1. Since reproducibility of results was of interest, some duplicate runs were made and the agreement of results was noted. Sample duplicate runs are shown in figures 11(a) and 11(b) for n-hexane and n-heptane, respectively.

The effect of different air temperatures on the temperature and radius histories are shown in figures 12(a) and 12(b) for isooctane and n-decane. The velocity of the air varied between narrow limits as shown in the figures. This variation in velocity produces a negligible effect on the wet-bulb temperatures. As would be expected, as the air temperature increases the rate of vaporization increases, thereby decreasing the length of time required to vaporize a given percentage of the mass of the drop. This reduction in vaporization time was also accompanied by a reduction in the time duration of the unsteady state so that the ratio of the duration of the unsteady state to the total vaporization time remained approximately constant.

It can also be seen in figure 13 that the relationship between the wet-bulb temperature and air temperature is not linear and that the wet-bulb temperature increases more slowly at the higher air temperature. The fuel used also plays an important part in the vaporization process. To illustrate this, figures 14(a) and 14(b) show a variety of fuels at both a low and a high air temperature, respectively. The fuels were initially at their room wet-bulb (and therefore slightly different) temperatures. It will be noted that at low air temperatures there is a ratio of about 3 to 1 for the vaporization times of n-decane and n-hexane, while at the high air temperatures this ratio is reduced to approximately 1.5 to 1. This indicates that at the high air temperatures encountered during combustion the total vaporization times of drops of different fuels will not be so markedly different as at low temperatures. This is due to the fact that the curves of vapor pressure at the wet-bulb temperatures against air temperatures must all converge to the value of the total pressure for the different fuels at high air temperatures as shown in figure 15

or, putting it another way, at extremely high air temperatures the wet-bulb temperature approaches the boiling temperature. These statements should not be construed to mean that fuel volatility is unimportant but merely that it is more important at low than at high air temperatures.

Very little work was done on the effect of drop size on vaporization. However, figures 16(a) and 16(b) show the results obtained for n-hexane and n-decane, respectively, when different-sized drops were used. These runs were all made at one air condition and therefore differences in the results shown should be entirely due to size differences.

Binary Mixtures

As a matter of interest, temperature histories of a few binary mixtures of hydrocarbons were obtained experimentally.

Experimental temperature histories of mixtures of n-octane and n-heptane and of n-octane and cetane with compositions by volume of 25, 50, and 75 percent were obtained. None of these mixtures gave or would be expected to give constant wet-bulb temperatures such as those obtained with drops of pure hydrocarbons.

The n-heptane – n-octane system (fig. 17(a)) gave steadily rising wet-bulb temperatures. The slope of the "steady-state" line became greater as the original percentage of the heavier, less volatile component (n-octane) in the mixture was increased.

The n-octane – cetane system (fig. 17(b)) showed a different characteristic. These drops tended to reach a "pseudo" steady state; that is, the temperature-time curve showed a tendency to level off after the initial rise. This tendency is more pronounced the greater the percentage of the more volatile component (n-octane). This produces an S-shaped wet-bulb region rising finally and leveling off at the wet-bulb temperature of pure cetane. This temperature, under the conditions of the experiment, was close to the temperature of the air. Figure 17 also shows experimental temperature-time histories of drops of pure n-heptane, n-octane, and cetane for comparison purposes.

Burning Drops

Again as a matter of interest, temperature histories were obtained for drops suddenly exposed to air at such high temperatures that combustion occurred. The resulting curves for different fuels are shown in figure 18.

The curves of figure 18 were obtained in the following manner. Products of combustion from an acetylene-air torch were passed through a 15-inch section of a 2-inch pipe. Excess air was drawn in the pipe by convection and venturi effects. The drop was hung about 1 inch above the top of this pipe and could be swung over the hot gases when desired. A Chromel-Alumel thermocouple was used. It was found experimentally that the drops would not burn until the temperature of the mixture of the products of combustion and air reached about 1,400° F.

It was also noticed during the experiments that the burning drops of different fuels varied markedly in their tendency to drop off the thermocouple. In general, the higher the molecular weight the greater the tendency to drop off the thermocouple. This may merely reflect the fact that the wet-bulb temperatures were higher for the higher molecular weight fuels. It was also noticed that occasionally spots on the surface seemed to boil which indicates that the heat transfer by radiation or conduction through the wires was not negligible, since according to the theory presented in reference 1 when the drop is receiving heat from the air only the wet-bulb temperature should approach but not reach the boiling temperature.

For these experiments the thermocouple and recorder were not calibrated and it was impossible to determine with precision if the drops reached exactly the boiling temperatures. The recorded thermocouple temperature, however, was very close to the boiling temperature and the wet-bulb values were arbitrarily shown in figure 18 as the boiling temperatures of the fuels. The amount of heat transfer by conduction down the thermocouple wire and by radiation to the thermocouple were not evaluated.

Since the lifetime of the burning drop was short the speed of response of the recorder is of interest. The dashed line in the upper left-hand region of the figure shows the response of the recorder to a step voltage.

DISCUSSION

The purpose of the present investigation was (1) to establish the importance of the unsteady-state portion of the vaporization time of fuel drops in hot air experimentally and (2) to determine whether temperature and mass histories of these vaporizing drops could be accurately predicted from the theory.

The importance of the unsteady state as a major portion of the time elapsed before ignition occurs in continuous-flow combustion chambers has been suggested theoretically (ref. 1). The existence and importance of the unsteady state has also been shown in all the experimental histories

presented in this report. Thus the authors accept it as a fact that the unsteady state should not be neglected in any detailed calculations. The magnitude of the error involved in neglecting it will be discussed later.

Circulation in Drops

In attempting to correlate calculated and experimental results, an investigation of the various assumptions and correlations used in the theory seemed necessary. The first assumption to be checked was that of infinite thermal conductivity of the liquid since, in all of the calculations performed in this project, this value was assumed to be infinite. The drop was thus assumed to be at a uniform temperature at all times. If this were not true experimentally, that is, if the drop had finite liquid conductivities, the thermocouple whose junction is, on the average, embedded at some point between the center and the surface of the drop might read a temperature lower than that existing at the surface of the drop. The temperature read from the thermocouple would also be lower than the temperature calculated with the assumption of infinite thermal conductivity.

The validity of the assumption of infinite thermal conductivity was estimated (ref. 1) by the use of the Gurnie-Lurie charts and the possibility of temperature gradients was indicated. It was pointed out, however, that the Gurnie-Lurie charts are based on assumptions not applicable to a vaporizing liquid drop and that the result of this analysis should be regarded as relative only.

Since there was some question about the applicability of the Gurnie-Lurie charts, theoretical calculations for the case of a drop of n-octane using finite values of thermal conductivity were undertaken (see appendix A). The results of the calculations show the temperature histories of four segments (see fig. 19) within the drop. In figure 20 these temperatures are compared with the temperature as calculated with the assumption of infinite thermal conductivity. Figure 20 would predict a large difference between theory and experiment if the assumption of infinite thermal conductivity were incorrect, since in the experiments the thermocouple junction normally lies somewhere between segments II and III of the drop. In the case for which the computations were performed the thermocouple would thus read temperatures as much as 30° to 40° lower than those predicted by using infinite thermal conductivities.

Since both of the above estimations indicated the presence of a temperature gradient in the drop, the experiments which were described earlier were conducted to investigate the existence of a temperature gradient within the drop. The data of figure 5 show that no detectable temperature gradients exist in a drop vaporizing in air under the conditions of the experiment.

Internal circulation in the vaporizing fuel drops was observed and photographed as explained previously (figs. 6 to 8). The motion pictures in the film supplement show the following facts:

(1) n-Octane drops show very slow internal circulation in still room air at 70° F. The direction of motion of the fluid in this case is downwards near the surface and upwards near the center in a doughnut-shaped pattern as shown in fig. 8(a).

(2) Cetane drops show even slower fluid motion in still room air. The direction of motion in this case, however, is essentially random.

(3) All the drops studied showed a rapid internal circulation when subjected to an air stream. The direction of the motion was reversed and was upwards near the surface and downwards near the center (fig. 8(b)). The direction of the air stream was upwards.

Three representative frames taken with the slow-speed camera are reproduced in figure 6. Figure 6(a) shows the aluminum-oxide particles in a drop of n-octane hanging in still room air. This frame was taken with a camera speed of 64 frames per second. Figure 6(b) shows a drop under similar air conditions but taken with a camera speed of 16 frames per second. The streak effect due to particle motion at longer exposure times is made evident by comparing figures 6(a) and 6(b). Figure 6(c) shows a cetane drop hanging in a stream of air at 250° F and velocity of 6 feet per second. This picture was taken with a camera speed of 64 frames per second. The motion of the aluminum-oxide particles was so much faster that they could not be stopped by using this camera speed, but the lobe or path of the particles is clear from this picture.

The high-speed pictures permitted an approximate evaluation of the speed of the particles inside a 2,000-micron-diameter cetane drop. Maximum velocities of 2 inches per second were observed when the air velocity was 6 feet per second. Particles were found to complete a cycle in approximately 1/8 second.

It was concluded from this photographic study that, under conditions similar to those used in the experiments, internal circulation exists in vaporizing drops in a magnitude that causes sufficient mixing of the fluid to eliminate temperature gradients during the heating-up period. This is in agreement with the results of the three-thermocouple experiment (fig. 5). This circulation is presumably caused by the skin drag of the stream of air passing by the drops. The circulation increases with airspeed, and the direction of motion of the dust particles near the surface of the drops is the same as that of the air. In still room air the direction of motion of these particles in an n-octane drop is reversed in direction from that which occurs when the drop is in an upward air stream; that is, it is downwards near the surface. This apparently is caused by evaporation of

the heavier-than-air n-octane vapor which, combined with the cooling effect, would cause a downward air current causing drag in that direction. In a cetane drop, the motion was slow and random because cetane has an extremely low vapor pressure and high liquid viscosity at the temperature of the room air (80° F). The slow and random motion inside the cetane drop was possibly caused by random air currents. This circulation explains the apparent infinite thermal conductivity observed experimentally when using three thermocouples in one drop.

There is an interesting correlation between internal circulation and the results of the experiments using binary mixtures. It was found that the n-octane – n-heptane drop showed a steadily rising wet-bulb temperature (fig. 17(a)). Since liquid diffusion is relatively slow it is thought that if there were no internal mixing due to circulation a constant ratio of the components (equal to the ratio of each component in the original mixture) would always evaporate from the surface of the drop. Therefore, if there were no circulation a constant wet-bulb temperature having a value falling somewhere between the wet-bulb temperature of the pure compounds at the same air temperature and pressure should result. However, since circulation and mixing take place, the more volatile component will be able to diffuse out through the film at a higher rate than the less volatile component with the exact relative rates being dependent upon the volatility and diffusion coefficients of the two components. Consequently, the drop will continuously and steadily change composition and will become more and more rich in the lower volatility component. Thus a rising wet-bulb temperature will result as is shown by the experimental data presented in figure 17(a).

It has been pointed out (ref. 3) that for constant conditions the internal circulation inside a drop decreases with drop size. It has also been pointed out that it is affected by the external Reynolds number as well as by the liquid and air viscosities. Since under conditions of interest in jet-engine combusion chambers the ratios of the drop velocities to the air velocities are of greater magnitudes than those used in the experiment, circulation may still exist in drop sizes of interest in a jet engine. While it is admittedly an opinion the authors feel that the assumption of infinite thermal conductivities within the liquid drops is a valid assumption for small drops as well as for large drops.

There is also one other interesting possible effect of circulation. It has been suggested (ref. 6) that circulation in the drop may cause a change in the film thickness and thus affect the heat and mass transfer. The authors have done no work that would either prove or disprove this suggestion.

Comparison of Experimental and Calculated Curves

As previously mentioned, one purpose of the investigation was to determine if temperature and mass histories of drops could be accurately predicted from theory. Having established that the heat transfer down the thermocouple was small and that the effective thermal conductivity of the liquid was high, a comparison between experimental and calculated results could be made.

In making this comparison it should be remembered that the theory for vaporizing drops has not been well worked out. In fact, the entire field of simultaneous heat and mass transfer has not been well studied from a theoretical standpoint. Appendix B presents an attempt to start from fundamental considerations and to establish and specify clearly any simplifying assumptions made in obtaining usable equations. The new theory is not complete, but it does present results of the theoretical work done to date. Since the theory is in a state of flux, it will be noted that the new theory presented in appendix B is not in complete agreement with that used for the calculations in this report. It is hoped that further work will clearly establish the fundamental considerations and form of equations involved.

Figure 21 presents curves of wet-bulb temperature versus air temperature. The calculated curve was obtained by using the procedure as outlined in reference 1 and the form of correlation specified in appendix B. It is seen in figure 21 that, if the proper choice of the diffusion coefficient is made, the agreement between calculated and experimental temperature histories is within the experimental error.

Figure 22(a) presents data showing a comparison of experimental rates of mass transfer and calculated rates of mass transfer. These mass-transfer rates were evaluated at corresponding points during the steady-state portion of the temperature history. Again the agreement is within the experimental error.

Figure 22(b) presents another comparison of experimental and calculated mass-transfer rates. For this comparison the calculated mass-transfer rates were determined from the experimental temperature histories rather than from the calculated temperature histories. There is an indication in figure 22(b) that the mass-transfer equations do not have the correct temperature dependency. However, the difference between the calculated and experimental temperature histories is hardly more than the experimental error and probably no conclusion should be drawn until data are obtained at higher air temperatures. These data emphasize the fact that a small difference in the temperature histories makes a fairly large difference in the mass histories.

Figure 23 presents a comparison of calculated and experimental temperature, mass, and radius histories. The comparisons are made at the

two extremes of air temperatures used and for the two extremes of fuels used with respect to volatility. Again the agreement is not perfect but is reasonably good.

It should be pointed out that the experimental and calculated curves presented in this report are for a constant droplet velocity relative to the air throughout their lifetime. This has been necessitated by the difficulty in adjusting the rate of air flow past the drops experimentally to conform to exact velocities existing in a combustion chamber. The conclusions arrived at in this report as to the effect of different parameters on the relation of calculated and experimental histories are, however, valid. The effect of a change in the relative velocity of drop and air due to aerodynamic drag has been investigated theoretically in reference 1.

Effect of Different Factors on Calculated Results

As has been explained in the previous section, while the agreement is not perfect between experiment and theory, the agreement is probably within the limits of error of the theory and experiment. As is also explained in appendix B some of the factors used in the theory are not firmly established, but it was felt of interest to see the effects of omitting or including certain factors.

The Ranz and Marshall heat- and mass-transfer correlations (see appendix B) were used for the present calculations as well as those of reference 1. The theory developed in reference 1 suggests that correction factors should be used when the mass transfer is high. Although the new theory presented in appendix B suggests that the correction factors used are incomplete, they were used in the present computations and it is of interest to see the effect of their omission.

The Z factor (ref. 1) represents that fraction of the total heat transfer from the air that finally arrives at the surface of the liquid drop. The balance of the heat is carried back with the diffusing vapor in the form of superheat. In the mass-transfer equation, α represents a correction factor that corrects an equimolal rate to unidirectional conditions (ref. 1).

The effect of the inclusion of each and both of these factors on the temperature and mass histories of vaporizing drops is illustrated in figure 24. This figure presents the histories of temperature, mass, and percent of total mass transferred for a drop of n-octane for the following cases:

(1) Experimentally determined

(2) Calculated with both the α and Z factors included in the equations

(3) Calculated with both the α and Z factors omitted from the equations

(4) Calculated with Z alone omitted from the heat-transfer equation

(5) Calculated with α alone omitted from the mass-transfer equation

It can be seen from these plots that the omission of both the α and Z factors from the equations yielded wet-bulb temperatures and mass-transfer rates that were higher than those experimentally determined. The omission of the Z factor alone yielded lower wet-bulb temperatures than those obtained with both α and Z omitted but still higher than those experimentally determined, plus a high mass-transfer rate. The omission of α alone yields temperature and mass histories that are closer to those experimentally determined than the previous two cases but not materially better than those calculated with both α and Z included in the equations. It is the opinion of the authors that at least until more work is done both the Z and α factors should be included at all times.

The physical properties of the air and hydrocarbons under question are given in various sources in the literature (refs. 7 to 12). It was beyond the scope of the present studies to determine which of the sources gave data that fit the hydrocarbons under test more closely. Reference 13 lists the different sources of the physical properties that were used in the computations together with the equations that were fit to these properties to allow their automatic computation at different temperatures by the IBM machines.

The new theory of appendix B suggests that the values of the thermal conductivity and diffusion coefficient should be determined at the temperature of the liquid. The values used in the calculations of reference 1 and in this report were average values for the film.

Figure 25 presents computed results when the physical constants were evaluated at two different temperatures – one the arithmetic mean temperature of the film and the other the temperature of the air. It can be seen that the choice of the temperature at which the properties are evaluated does not have a marked influence on the computed curves.

The method employed to determine the diffusion coefficient does affect the results very markedly, however. Figure 26 shows the effect on the calculated curves of using different techniques for determining the diffusion coefficient. In these calculations the diffusion coefficient was determined by the three techniques described by Hirschfelder, Curtiss, and Bird (ref. 11). In these three different techniques the intermolecular force constants of the fuels were determined in three different ways:

(1) From critical constants of the fuel

(2) From experimentally determined second-virial coefficients

(3) From experimental values of the viscosity

A large variation between results is observed. If Gilliland's equation (ref. 14) were used even more of a variation would be found. Since Gilliland's equation gives a smaller diffusion coefficient at high temperatures and hence a slower vaporization rate than the diffusion coefficients of Hirschfelder, Curtiss, and Bird it was not used.

Because of this rather large variation in the value of the diffusion coefficient (and thus in the calculated vaporization rate) it was decided to use a single technique for calculating diffusion coefficients. Since figure 26 indicates that the diffusion coefficients from viscosity data are probably too small and since experimental information was not available for either the second-virial coefficient or for the viscosity for all hydrocarbons, it was decided that the diffusion coefficients would be evaluated from the critical constants. It should be noted, however, that the diffusion coefficients determined from critical data are considered by Hirschfelder, Curtiss, and Bird to be less reliable than those obtained by other techniques. By using the highest computed value for the diffusion coefficient, the use of the correlations of Ranz and Marshall in the computations produced curves that agreed reasonably well with the experimental curve.

Both in the calculations of reference 1 and in the material presented in this report thermal diffusion has been neglected. It was neglected because of the complexity introduced by its use and because of the feeling that its contribution was small. Since as the temperature difference between the drop and the air increases the effect of thermal diffusion may not be negligible, an estimation was made of its effect. At a temperature of $1,073^{\circ}$ R it was estimated that the thermal diffusion reduced the vaporization rate by 8 percent. Thus while the effect of thermal diffusion has not been large in the present report it probably should be included in any additional work done at higher temperatures.

Factors Affecting Lifetime of a Drop

It was considered of interest to attempt to estimate the relative magnitude of the factors affecting the lifetime of a drop. However, in making this estimation it will be necessary to make numerous simplifications and the estimation will therefore of necessity be of limited value.

The three primary factors affecting the lifetime of a drop are:

(1) The condition of the ambient air, that is, velocity, pressure, and temperature

(2) The fuel used and its properties, that is, vapor pressure, diffusion coefficient, thermal conductivity, and so forth

(3) The initial condition of the drop, that is, temperature, size, and so forth

These factors are all tied together by the heat- and mass-transfer equations

In order to make an estimation of the relative effects of the variables the following assumptions will be made:

(1) The drop is in the steady state for its entire lifetime. The magnitude of the error in this assumption will be discussed later.

(2) The conditions of the air surrounding the drop are constant; this includes the pressure, temperature, and velocity of the air.

As has been discussed in appendix B, the theory for a vaporizing drop has not been completely worked out. However, the data previously presented in this report show reasonably good agreement between the theory presented in reference 1 and the experiment. Thus this theory will be used for the present estimation. The equations for the lifetime of a drop have been derived in appendix C for the two limiting cases of zero air velocity and large Reynolds number and for the general case.

The equation for the lifetime of a drop at zero air velocity, that is, a drop evaporating in still air, shows that the lifetime is proportional to the square of the initial radius, to the liquid density, and to its latent heat of vaporization and inversely proportional to the thermal conductivity of the ambient atmosphere and its wet-bulb depression. Stating it another way, the lifetime of the drop is proportional to the square of its initial radius, its density, and the ratio of the latent heat of vaporization to the heat transfer to the drop.

When the Reynolds number is high, the lifetime of the drop is directly proportional to its latent heat of vaporization, its density, and its initial radius to the 1.5 power. It is also inversely proportional to the difference between the wet- and dry-bulb temperature. In this connection it will be noted that the wet-bulb temperature can be estimated from equation (26) of reference 1. It will also be noted that Ingebo (ref. 15) obtained relationships similar to equations (C10)

and (C13) (appendix C). However, because of his use of a slightly different correlation he found that θ_t varied as the 1.4 power of the radius at high Reynolds numbers.

Equation (C14) (appendix C) shows the lifetime of a drop in the case where the velocity is neither zero nor extremely high. Unfortunately, the relationship does not reduce to a simple form such as the forms for the two limiting cases.

While equations (C10), (C13), and (C14) provide some insight into the factors affecting the lifetime of a drop, the relationships are still perhaps not readily visualized. Figure 27 presents experimental data on the lifetime of drops and may help to show general trends. It should be noted that the time plotted is the time for 80-percent vaporization rather than for complete vaporization.

Figure 27(a) presents data on the time required for 80-percent vaporization as a function of the fuel used with lines of constant temperature. At low temperatures the dependence of the lifetime of the drop on fuel is rather marked, while at higher temperatures the dependence is less marked. All the fuels shown in figure 27(a) are normal paraffins except for isooctane.

Figure 27(b) presents the time for 80-percent vaporization as a function of air temperature and is simply a cross plot of figure 27(a). As a matter of interest the data on burning drops were included in the plot. The value shown for the air temperature is undoubtedly incorrect since the drops were burning and the drop size may not have been the same, but the data were included to show the trend. Again, the data show that the effect of fuel on the lifetime of a drop is of lesser importance at the higher temperatures.

It will also be noted that while drop size has a major effect on the lifetime of a drop it is probably because the radius can be varied over such wide ranges. For example, the drop radius can be varied over a 100 to 1 range. It would be rather difficult, if not impossible, to change the other variables over such a wide range.

Figure 28 presents data that were calculated in an attempt to show the effect of neglecting the time spent in the unsteady state. The curve for "infinite thermal conductivity" was calculated in the usual manner as outlined in this report and represents a good approximation to the actual history of the drop. The curve for "no unsteady state" was computed under the assumption that the drop was mysteriously but instantaneously raised to its wet-bulb temperature. The third curve for "zero thermal conductivity" was calculated under the assumption that the thermal conductivity of the liquid was zero and the fuel came off in layers.

As can be seen in figure 28, the assumption that the thermal conductivity of the liquid is zero results in a rate of mass transfer that is initially too high but eventually becomes less than that of the actual case. On the other hand, the assumption of no unsteady state gives values of mass transfer that are too high at all times.

The error in time varies as the percent mass transferred is varied. For example, if the item of interest is the time required to vaporize 20 percent of the mass, the error can be 100 percent or more. On the other hand, if the item of interest is the time required to vaporize 80 percent of the mass, the error may be more of the order of 20 percent.

University of Wisconsin,
Madison, Wis., May 2, 1954.

APPENDIX A

THEORETICAL CALCULATION FOR UNSTEADY STATE WITH FINITE LIQUID THERMAL CONDUCTIVITY

Vaporization histories during the unsteady state are presented here with the assumption of finite thermal conductivities within the drop. To make these calculations feasible, the drop was divided into three shells of equal initial thickness plus a spherical core of twice that thickness (fig. 19). Thus the radius of the drop was divided into four initially equal segments having a thickness x.

The following assumptions were made:

(1) Each of the segments had a uniform temperature at any instant equal to the mean temperature at its center line T_{m_1}, T_{m_2}, and so forth corresponding to segments 1, 2, and so forth. These were also time-average temperatures for any time increment in the stepwise procedure used.

(2) The drop surface temperature was assumed to be that of the outer shell T_{m_1}.

(3) The inner segments remained at the same thickness x. The outer segment had a varying thickness x_1 because of (a) vaporization and (b) liquid diffusing to it from the inner segments because of thermal expansion.

(4) The liquid specific heats c_{pL1}, c_{pL2}, and so forth and the liquid densities ρ_{L_1}, ρ_{L_2}, and so forth, corresponding to segments 1, 2, and so forth were derived at any instant at mean temperatures T_{m_1}, T_{m_2}, and so forth of the segments.

(5) The thermal conductivities of the segments were computed at the borderlines between segments 1 and 2, 2 and 3, and so forth at temperatures equal to the average value between T_{m_1} and T_{m_2}, T_{m_2} and T_{m_3}, and so forth, thus giving conductivities K_{12}, K_{23}, and so forth.

The calculations were performed by specifying an increment in surface temperature or specifying T_{m_1} and then assuming the temperatures T_{m_2}, T_{m_3}, and T_{m_4}. The time increment $\Delta\theta$ for that temperature

increment together with the radius r_o and the velocity V_2 at the end of the increment were also assumed. The value of sensible heat arising at the surface of the drop was then calculated in the usual manner described in reference 1 by evaluating the fuel vapor pressure at the surface temperature T_{m_1}. The following equations were then used to calculate the temperature increment of each segment ΔT_1, ΔT_2, and so forth for the assumed time increment $\Delta\theta$.

For the first segment:

$$\Delta T_1 = \frac{Q_L - Q_{o1}}{m_1 c_{pL1}} \Delta\theta$$

$$= \frac{Q_L - \left(T_{m1} - T_{m2}\right) \frac{K_{12}}{\frac{1}{2}\left(x_1 + x\right)} 4\pi(3x)^2}{\frac{4}{3}\pi\left[r_o^3 - (3x)^3\right]\rho_{L_1} c_{pL1}} \Delta\theta \qquad \text{(A1)}$$

For the second segment:

$$\Delta T_2 = \frac{Q_{o1} - Q_{o2}}{m_2 c_{pL2}} \Delta\theta$$

$$= \frac{Q_{o1} - \left(T_{m2} - T_{m3}\right) \frac{K_{23}}{x} 4\pi(2x)^2}{\frac{4}{3}\pi\left[(3x)^3 - (2x)^3\right]\rho_{L_2} c_{pL2}} \Delta\theta \qquad \text{(A2)}$$

For the third segment:

$$\Delta T_3 = \frac{Q_{o2} - Q_{o3}}{m_3 c_{pL3}} \Delta\theta$$

$$= \frac{Q - \left(T_{m3} - T_{m4}\right) \frac{K_{34}}{x} 4\pi x^2}{\frac{4}{3}\pi\left[(2x)^3 - x^3\right]\rho_{L_1} c_{pL3}} \Delta\theta \qquad \text{(A3)}$$

For the fourth segment:

$$\Delta T_4 = \frac{Q_{o3}}{m_4 c_{pL4}}$$

$$= \frac{Q_{o3}}{\frac{4}{3}\pi x^3 \rho_{L_4} c_{pL4}} \Delta\theta \qquad (A4)$$

In these equations Q_{o1}, Q_{o2}, and Q_{o3} are the sensible heats going out of segments 1, 2, and 3 and crossing the borders into segments 2, 3, and 4, respectively. The calculated values of ΔT_1, ΔT_2, and so forth are then added to the initial temperatures of the corresponding segments for the particular time increment under investigation and the value thus computed is compared with the assumed value of T_{m1}, T_{m2}, and so forth. Several unsuccessful attempts were usually made in this trial and error procedure before calculated values that agreed with the assumed values were discovered.

APPENDIX B

THEORY OF SIMULTANEOUS MASS TRANSFER AND HEAT TRANSFER

As has been previously noted, the theory used in reference 1 has been used in the present report. The theory together with the correlation of Ranz and Marshall (ref. 12) have given reasonably good agreement with experiment. At the same time, there are certain ambiguities and inconsistencies in the correlations and theories and as a result some work has been done in an attempt to develop more fully the theory of simultaneous mass transfer and heat transfer.

For the sake of completeness the theory developed in reference 1 is summarized in a slightly modified form in this appendix together with additional but incomplete work done on the theory.

Mass Transfer

Summary of theory presented in reference 1.- For the case of a vaporizing liquid droplet where essentially unidirectional diffusion exists the following diffusion equation is given in reference 16:

$$\frac{dp_f}{dr} = -\frac{RT}{D_v P_T} r_f p_a \tag{B1}$$

For a spherical drop the molal rate of diffusion per unit area r_f must vary throughout the film and therefore cannot be treated as a constant as is done for two-dimensional diffusion. By defining the molal rate of diffusion per unit area at the liquid surface as r_{f_o} one obtains for spherically symmetrical diffusion

$$r_f = r_{f_o} \frac{r_o^2}{r^2} \tag{B2}$$

Combining these two equations and carrying out mathematical steps and substitutions as indicated in reference 1, one obtains:

$$w = \frac{D_v A_o}{\left(R/M_f\right) T_m} \left(\frac{1}{B_o} + \frac{1}{r_o}\right) p_{fL}{}^{\alpha} \tag{B3}$$

On a semiempirical basis the diffusion rate is customarily given as (ref. 16)

$$w = A_o K_g p_{fL} \alpha \tag{B4}$$

where K_g is the coefficient of mass transfer which can be determined from the following equation given by Ranz and Marshall for a liquid drop (ref. 12):

$$K_g = \frac{D_v}{2r_o\left(R/M_f\right)T_m} N_{Nu}' \tag{B5}$$

By combining the above three equations:

$$\frac{1}{B_o} + \frac{1}{r_o} = \frac{1}{r_o}\frac{N_{Nu}'}{2} \tag{B6}$$

With everything constant but the velocity of the air,

$$B_o = \frac{C_1}{\sqrt{U}}$$

Here the film thickness B_o for mass transfer is inversely proportional to the square root of the relative velocity of the droplet and air. While this film concept is, of course, used as an analysis and visualization aid rather than as an exact representation of the facts, it is interesting to note that B_o becomes large in still air and rapidly decreases to values of the order of the droplet radius and less as soon as a relative motion of air to drop takes place.

Analysis using "transport" theory.- If the mass transfer is analyzed according to "transport phenomena" based on the kinetic theory of dilute gases and thermodynamics of irreversible processes as described in reference 11, the transport of mass is dependent on: (1) A gradient in the chemical potential, (2) a gradient in the total pressure, (3) a gradient in the temperature of the gas, and (4) transport due to external forces.

For the case of a vaporizing drop the total pressure is constant and there are no external forces. There is a gradient in the temperature but its effect will be small and will be neglected in the present development. Thus, considering only the transport of mass per unit area dA due to a gradient in the chemical potential, the flux equation is

$$j_i = n_i m_i d_{vi} \tag{B7}$$

For a two-component system the flux vector with respect to the mass average velocity is:

$$j_i = \frac{n^2}{\rho_n} m_1 m_2 D_v \nabla \frac{n_i}{n} \tag{B8}$$

For a vaporizing drop the vector of interest is the flux vector with respect to the liquid surface. At the liquid surface the velocity of the air is equal to the surface velocity. To convert the above equations to corresponding terms with respect to component 2 (the air) the following terms are used:

F_1 mass flux vector of component 1 with respect to velocity of component 2

V_{d1} velocity of component 1 with respect to velocity of component 2

$$V_{d1} = d_{v1} - d_{v2}$$

$$F_1 = n_1 m_1 V_{d1} = n_1 m_1 (d_{v1} - d_{v2})$$

From momentum considerations,

$$n_1 m_1 d_{v1} + n_2 m_2 d_{v2} = 0$$

therefore

$$d_{v2} = - d_{v1} \frac{n_1 m_1}{n_2 m_2}$$

Then

$$F_1 = n_1 m_1 d_{v1}\left(1 + \frac{n_1 m_1}{n_2 m_2}\right)$$

$$= \frac{n^2}{\rho_n} m_1 m_2\left(1 + \frac{n_1 m_1}{n_2 m_2}\right) D_v \nabla \frac{n_1}{n}$$

$$= \frac{n^2}{\rho_n} m_1 m_2\left(\frac{n_1 m_1 + n_2 m_2}{n_2 m_2}\right) D_v \nabla \frac{n_1}{n}$$

$$= \frac{n^2}{\rho_n} m_1 m_2 \frac{\rho_n}{n_2 m_2} D_v \nabla \frac{n_1}{n}$$

$$= \frac{m_1}{n_2} n^2 D_v \nabla \frac{n_1}{n} \tag{B9}$$

For engineering calculations it is usually more convenient to use the flux as defined by

$$f_1 = \frac{F_1}{M_1}$$

or

$$f_1 = \frac{m_1 n^2}{M_1 n_2} D_v \nabla \frac{n_1}{n}$$

For an ideal gas

$$\frac{n_i}{n} = \frac{p_i}{P_T}$$

and

$$\frac{m_i n_i}{M_i} = \frac{p_i}{RT}$$

therefore

$$\frac{m_i n}{M_i} = \frac{P_T}{RT}$$

where p_i is the partial pressure of component i; then

$$f_1 = \frac{P_T}{RT} \frac{n}{n_2} D_v \nabla \frac{p_1}{P_T}$$

and, for constant total pressure,

$$f_1 = \frac{n}{n_2} \frac{D_v}{RT} \nabla p_1$$

$$= \frac{P_T}{p_2} \frac{D_v}{RT} \nabla p_1 \tag{B10}$$

If there is no pressure gradient of the liquid vapor tangential to the liquid surface, and if the drop is spherical, this reduces to

$$f_1 = \frac{P_T}{p_2} \frac{D_v}{RT_L} \left(\frac{\partial p_1}{\partial r} \right)_{r=r_o} \tag{B11}$$

To obtain the total mass flow from the drop, integration is taken over the entire surface, or:

$$w = \int_R f_1 \, dA = \int_R \frac{P_T}{p_2} \frac{D_v}{RT_L} \left(\frac{\partial p_1}{\partial r} \right)_{r=r_o} dA$$

If the total pressure, partial pressure of component 2, D_v, R, and T_L are all constant over the entire surface,

$$w = \frac{P_T}{p_2} \frac{D_v}{RT_L} \int_R \left(\frac{\partial p_1}{\partial r} \right)_{r=r_o} dA \tag{B12}$$

It is convenient to define a reduced pressure, reduced area, and reduced radius as:

$$p_1^* = \frac{p_1}{p_{fL} - p_{fb}} \tag{B13}$$

$$A^* = A/A_o$$

and

$$r^* = \frac{r}{2r_o} \tag{B14}$$

therefore,

$$w = A_o \frac{P_T}{p_2} \frac{D_v}{RT_L 2r_o}(p_{fL} - p_{fb}) \int_R \left(\frac{\partial p_1^*}{\partial r^*}\right)_{r=r_o} dA^* \tag{B15}$$

where it is understood that the reduced pressure gradient and all the other terms are to be evaluated at the liquid surface. The integral $\int \frac{\partial p_1^*}{\partial r^*} dA^*$ for mass transfer is similar to the integral of Schlichting (ref. 17) obtained for heat transfer. He called it the Nusselt number for heat transfer. It will be defined here as the Nusselt number for mass transfer, or

$$N_{Nu}' = \int_R \left(\frac{\partial p_1^*}{\partial r^*}\right)_{r=r_o} dA^* \tag{B16}$$

Equation (B15) together with the definition of the Nusselt number is the fundamental equation for mass transfer. Its limitations are:

(1) Total pressure is assumed constant

(2) Thermal diffusion and external forces are neglected

(3) The drop is spherically symmetrical in all respects

In general, equation (B15) has not been used explicitly to evaluate mass transfer since values for the Nusselt number can be obtained only from experimental data. Thus, by analogy with heat transfer, an empirical equation of the form

$$w = K_g A_o \left(p_{fL} - p_{fb} \right) \tag{B17}$$

is customarily used in practical calculations with the mass-transfer coefficient being defined by the equation itself. It has also been recognized that there is a difference between equimolal and unidirectional diffusion so that some authors have preferred to write

$$w = K_g A_o \alpha \left(p_{fL} - p_{fb} \right) \tag{B18}$$

where it is implied that K_g is the mass-transfer coefficient for equimolal diffusion. Here α is a correction factor that is greater than 1 for unidirectional diffusion and is determined by a procedure similar to that outlined previously in this section.

By dimensional analysis as suggested by Buckingham (ref. 18) the dimensionless group

$$\frac{K_g R T_L 2 r_o}{D_v} = N_{Nu}' \tag{B19}$$

can be developed when K_g is defined as in equation (B17). This dimensionless group has also been defined and set equal to the Nusselt number for mass transfer.

It can be seen by comparison of equations (B15) and (B19) that the Nusselt numbers as defined by equations (B16) and (B19) will be equal only in the case where P_T/p_2 is unity; that is, they will approach each other as the mass transfer approaches zero. Most of the experimental data in the literature have been taken where P_T/p_2 is essentially unity and it has not been clear nor has it made any difference whether this Nusselt number has been defined by equation (B16) or equation (B19). The authors currently feel that the best procedure from all standpoints is to define the Nusselt number as

$$N_{Nu}' = \int_R \left(\frac{\partial p^*}{\partial r^*} \right)_{r=r_o} dA^* \tag{B20}$$

and to define K_g under all conditions by the equation

$$w = K_g A_o \left(p_{fL} - p_{fb} \right)$$

The choice is admittedly arbitrary, but confusion had existed and does exist and will continue to exist until universal agreement is obtained for the definition of the Nusselt number and the mass-transfer coefficient K_g.

Also of interest in the light of the above theory is the significance of the α term used in the calculations for this report. Equations (B18) and (B19) were used. However, the Nusselt number correlations were obtained under conditions of extremely small pressure differences. This condition will be denoted by the superscript o for the previous derivation of the Nusselt number or

$$\left(N_{Nu'}\right)^{o} = \int_{R} \left(\frac{\partial p_1^*}{\partial r^*}\right)^{o}_{r=r_o} dA^* \tag{B21}$$

combining equations (B18), (B19), and (B21). Therefore,

$$w = A_o \frac{D_v}{2r_o RT_L}\left(p_{fL} - p_{fb}\right)\alpha \int_{R} \left(\frac{\partial p_1^*}{\partial r^*}\right)^{o}_{r=r_o} dA^* \tag{B22}$$

Comparing this with equation (B18) and solving for α:

$$\alpha = \frac{P_T}{p_2} \frac{\int_{R} \left(\frac{p_1^*}{r^*}\right)_{r=r_o} dA^*}{\int_{R} \left(\frac{p_1^*}{r^*}\right)^{o}_{r=r_o} dA^*} \tag{B23}$$

The above discussion has shown the relationship between the fundamental equation for the transfer of mass and the equations used in this report. If this fundamental equation is compared with the correlations of Ranz and Marshall, it would seem that the terms $M_m P_a/\rho_a$ should reduce to RT. The terms will not, of course, reduce to RT unless all the subscripts are the same. If the subscripts are not the same, some confusion exists as to the molecular weight to be used in converting moles to pounds. In the work done for the correlation the values M_m and M_a were usually nearly equal. In the work of reference 1 and this report there often is a major difference.

In the work of reference 1, M_f was used for M_m in the term $M_m P_a/\rho_a$. However, comparison with experiments soon showed that substituting RT for

$M_m p_a/\rho_a$ gave much better agreement with experiment and consequently RT has been used for this report.

It also follows that D_v should be evaluated at the temperature of the liquid surface. The above discussion does not, however, yield any clue as to the temperature at which the dimensionless parameters such as the Reynolds number could be evaluated, since this enters into the evaluation of $\int_R \left(\frac{\partial p^*}{\partial r^*}\right)_{r=r_o} dA^*$. For this report all properties, including D_v, were evaluated at the mean temperature of the film. More work is being done in an attempt to determine more clearly theoretically all the dimensionless terms that enter into the Nusselt number $\int_R \left(\frac{\partial p^*}{\partial r^*}\right)_{r=r_o} dA^*$ under all conditions.

Heat Transfer

Summary of theory presented in reference 1.- For spherically symmetric heat transfer the equation given in reference 1 for the total heat which arrives at the liquid surface in terms of the heat conducted through a thin layer of the film at radius r becomes:

$$Q_v = Q - Q_s$$

$$= 4K\pi r^2 \frac{dT}{dr} - wc_{pf}\left(T - T_L\right) \tag{B24}$$

By making the same assumptions and performing the mathematical steps as indicated in reference 1:

$$Q_v = K_m\left(\frac{1}{B_o} + \frac{1}{r_o}\right)4\pi r_o^2\left(T_B - T_L\right)\frac{z}{e^z-1} \tag{B25}$$

where the substitution for z is as follows:

$$z = \frac{wc_{pf}}{4\pi K_m}\frac{B_o}{r_o\left(r_o + B_o\right)} \tag{B26}$$

This z substitution is identical to that used in reference 1.

Performing an analysis similar to that given in the section "Mass Transfer," the following equation is obtained for the film thickness for heat transfer:

$$\frac{1}{B_o} + \frac{1}{r_o} = \frac{1}{r_o}\frac{N_{Nu}}{2} \tag{B27}$$

$$B_o = \frac{C_2}{\sqrt{U}}$$

It is interesting to note that equations (B6) and (B27) indicate that at other than zero velocity, where an infinite film thickness is indicated, a different film thickness is indicated for mass transfer and for heat transfer. According to the above equations, the two film thicknesses are in the ratio of the cube root of Schmidt to Prandtl numbers. This difference in film thickness has previously been suggested by Ackermann (ref. 19).

Analysis using "transport" theory.- From kinetic theory and thermodynamics of irreversible processes it is found that the transport of energy is dependent on: (1) A temperature gradient, (2) transport of thermal energy by the flux of molecules, and (3) the "reciprocal process" to thermal diffusion known as the "Dufour effect."

By neglecting the Dufour effect one obtains the following energy-flux equation for a two-component system in terms of a plane moving at the mass average velocity:

$$q = -K\nabla T + n_1 m_1 H_1 d_{v1} + n_2 m_2 H_2 d_{v2} \tag{B28}$$

To obtain the heat flux with respect to the liquid surface I, a transformation for velocities must again be performed. This transformation gives:

$$I = -K\nabla T + n_1 \dot{m}_1 H_1 V_{d1} \tag{B29}$$

Again, if there is no temperature gradient tangential to the liquid surface and if the drop is spherical at the liquid surface, this reduces to

$$I = -K\left(\frac{\partial T}{\partial r}\right)_{r=r_o} + n_1 m_1 H_1 V_{d1} \tag{B30}$$

To obtain the total energy transported to the liquid surface integrate over the entire liquid surface:

$$L = -KA_o \int \left(\frac{\partial T}{\partial r}\right)_{r=r_o} + A_o n_1 m_1 H_1 V_{d1} \tag{B31}$$

It is again convenient for dimensional analysis to define a reduced temperature as

$$T^* = \frac{T}{T_B - T_L} \tag{B32}$$

Then

$$L = -\frac{KA_o}{2r_o}\left(T_B - T_L\right) \int_R \left(\frac{\partial T^*}{\partial r^*}\right)_{r=r_o} dA^* + A_o n_1 m_1 H_1 V_{d1} \tag{B33}$$

The energy L arriving at the liquid surface does not include the work done by the moving boundary. Including this work in the energy balance for the system, one obtains:

$$L = A_o n_L m_L d_{vL} E_L + M_L \frac{dE_L}{d\theta} + pA_o V_L \tag{B34}$$

However,

$$A_o n_L m_L V_{dL} = \frac{dM_L}{d\theta} = -w$$

and

$$A_o p V_L = pV_L \frac{dM_L}{d\theta} = -pV_L w$$

Making these substitutions, combining equations (B33) and (B34), and rearranging give:

$$-\frac{KA_o}{2r_o}\left(T_B - T_L\right) \int_R \left(\frac{\partial T^*}{\partial r^*}\right)_{r=r_o} dA^* =$$

$$-w\left[\left(E_L + pV_L\right) - H_1\right] + M_L \frac{dE_L}{d\theta} \tag{B35}$$

If one combines $(E_L + pV_L)$ as H_L and uses the usual definition of the latent heat of vaporization λ as $(H_i - H_L)$ he obtains

$$-\frac{KA_o}{2r_o}(T_B - T_L)\int_R \left(\frac{\partial T^*}{\partial r^*}\right)_{r=r_o} dA^* = w\lambda + M_L \frac{dE_L}{d\theta} \tag{B36}$$

The right-hand side of this equation has been defined previously as Q_v or the heat arriving at the drop surface; that is

$$Q_v = \frac{KA_o}{2r_o}(T_B - T_L)\int_R \left(\frac{\partial T^*}{\partial r^*}\right)_{r=r_o} dA^* \tag{B37}$$

By definition

$$N_{Nu} = \int_R \left(\frac{\partial T^*}{\partial r^*}\right)_{r=r_o} dA^* \tag{B38}$$

then

$$Q_v = \frac{KA_o}{2r_o}(T_B - T_L)N_{Nu} \tag{B39}$$

Again, equation (B37) is the fundamental equation for heat transfer to the liquid surface. It assumes that:

(1) The Dufour effect is negligible

(2) The temperature difference between the liquid surface and the free air stream has a constant value

Also, again equation (B37) has not been used explicitly to evaluate heat transfer because of the difficulty in evaluating $\int_R \frac{\partial T^*}{\partial r^*} dA^*$, and an equation of the empirical form

$$Q_v = hA_o(T_B - T_L) \tag{B40}$$

has been used where the heat-transfer coefficient h was defined by the above equation. It has also been recognized that the presence of mass

transfer affects the heat transfer and some authors have then preferred the empirical equation

$$Q_v = hA_o\left(T_B - T_L\right)Z \tag{B41}$$

where Z was defined earlier and h was considered to be the heat transfer in the absence of mass transfer.

Reference 20 has shown that in the absence of mass transfer the Buckingham type of dimensional analysis will result in the dimensionless group

$$\frac{h2r_o}{K} = N_{Nu} \tag{B42}$$

where by definition the above dimensionless group was called the Nusselt number. This definition of the Nusselt number has been used in most experimental calculations. It is also true that most experimental correlations have been developed under conditions of either low or no mass transfer.

The value of the reduced temperature gradient $\int_R \left(\frac{\partial T^*}{\partial r^*}\right)_{r=r_o} dA^*$ depends upon whether or not mass transfer is present. It is also obvious from equation (B41) that the total heat transfer is not the same at the outer and inner edges of the film when mass transfer is present. Therefore for heat transfer in the presence of mass transfer it must be specified whether reference is made to the heat transferred to the outer or inner edge of the film. Thus when the empirically defined equation $Q = hA\Delta T$ is used in the presence of mass transfer it is necessary to specify whether Q is the heat transferred to the outer or inner edge of the film.

Again, confusion exists because of the lack of clear definition of terms. The author currently feels that it is most advantageous to define Q as the heat transferred through the inner edge of the film, that is, to the liquid surface, and to define h under all circumstances as

$$Q_v = hA_o\left(T_B - T_L\right)$$

The Nusselt number would then be defined as

$$N_{Nu} = \int_R \left(\frac{\partial T^*}{\partial r^*}\right)_{r=r_o} dA^*$$

and would implicitly be a function of whether mass transfer is present.

In connection with the above theory of the significance of the Z term used in the calculations (eq. (B41)) the Nusselt number used was defined by equation (B42); however, it was obtained under conditions of small simultaneous mass transfer. This condition will again be denoted by the superscript o for the Schlichting definition of the Nusselt number or

$$N_{Nu} = \int_R \left(\frac{\partial T^*}{\partial r^*}\right)^o_{r=r_o} \tag{B43}$$

Combining equations (B41) and (B42),

$$Q_v = \frac{KA_o}{2r_o}\left(T_B - T_L\right) Z \int_R \left(\frac{\partial T^*}{\partial r^*}\right)^o_{r=r_o} \tag{B44}$$

Comparing this with equation (B36) and solving for Z,

$$Z = \frac{\int_R \left(\frac{\partial T^*}{\partial r^*}\right)_{r=r_o}}{\int_R \left(\frac{\partial T^*}{\partial r^*}\right)^o_{r=r_o}} \tag{B45}$$

APPENDIX C

CALCULATION FOR LIFETIME OF A VAPORIZING DROP UNDER DIFFERENT AIR VELOCITIES

Equation (27) of reference 1 states that in the steady state the mass rate of vaporization is given by

$$w = -\frac{dM_L}{d\theta} = C_3 r_o \left(2 + C_4 r_o^{1/2}\right) \tag{C1}$$

where C_3 and C_4 are constants for a drop vaporizing in the steady state for any velocity condition. These constants have the following values:

$$C_3 = \frac{2\pi D_v}{r_f T} p_{fL} \alpha \tag{C2}$$

$$C_4 = 0.6\left(N_{Sc}\right)^{1/3}\left(\frac{N_{Re}}{r_o}\right)^{1/2} \tag{C3}$$

The mass of the drop M_L is

$$M_L = \frac{4}{3}\pi r_o^3 \rho_L$$

Therefore

$$dM_L = 4\pi\rho_L r_o^2 dr_o \tag{C4}$$

Combining equations (C1) and (C4) and rearranging them give

$$d\theta = -\frac{4\pi\rho_L}{C_3} \frac{r_o\, dr_o}{\left(2 + C_4 r_o^{1/2}\right)} \tag{C5}$$

Case I: Zero Velocity

If the limiting case where the velocity of the air with respect to the drop is zero is considered, then C_4 will be zero since it involves the velocity and equation (C5) reduces to

$$d\theta = -\frac{2\pi\rho_L}{C_3} r_o \, dr_o \tag{C6}$$

Integrating equation (C6) between $\theta = 0$ and $\theta = \theta_t$, the total vaporization time where $r_o = r_{ol}$, the initial drop radius, and $r_o = 0$ gives:

$$\theta_t = \frac{\pi\rho_L}{C_3}\left(r_{ol}\right)^2 \tag{C7}$$

Substituting for C_3 (eq. (C2)) gives

$$\theta_t = \frac{\rho_L r_f T}{2D_v p_{fL}\alpha}\left(r_{ol}\right)^2 \tag{C8}$$

Solving equation (26) of reference 1 for p_{fL} and changing the term $\left(\frac{p_a}{\rho_m}\right)$ to $r_f T$ (see appendix B) give

$$p_{fL} = \frac{r_f T K_m N_{Nu} Z}{D_v \lambda N_{Nu}' \alpha}\left(T_B - T_{as}\right) \tag{C9}$$

Noting that the term N_{Nu}/N_{Nu}' reduces to 1 at zero air velocity and combining it with equation (C8) give

$$\theta_t = \frac{\rho_L \lambda}{2K_m Z\left(T_B - T_{as}\right)}\left(r_{ol}\right)^2 \tag{C10}$$

Case II: High Reynolds Number

The other limiting case would be where the Reynolds number was quite high and the factor 2 in equation (C5) could be neglected. Under these circumstances equation (C5) reduces to

$$d\theta = -\frac{4\pi\rho_L}{C_3C_4}\left(r_o\right)^{1/2}dr_o \tag{C11}$$

Integrating equation (C11) between the same limits as in case I gives

$$\theta_t = \frac{8\pi\rho_L}{C_3C_4}\left(r_{ol}\right)^{1.5} \tag{C12}$$

Substituting values for C_3 and C_4 from equations (C2) and (C3) and for the Prandtl and Reynolds numbers and combining them with equation (C9) give

$$\theta_t = \frac{2.222\rho_L\lambda}{K_m Z\left(T_B - T_{as}\right)}\frac{K_m^{1/3}M_m^{1/6}}{c_{pm}^{1/3}\rho_m^{1/2}}\frac{1}{U^{1/2}}\left(r_{ol}\right)^{1.5} \tag{C13}$$

Case III: General Case

Integrating equation (C5) between the same limits as in cases I and II gives

$$\theta_t = \frac{8\pi\rho_L}{C_3C_4}\left[8\log_e\frac{2}{2 + C_4r_{ol}^{1/2}} + C_4r_{ol}^{1/2}\left(4 - C_4r_{ol}^{1/2} + \frac{C_4^2}{3}r_{ol}\right)\right] \tag{C14}$$

where C_3 and C_4 are defined by equations (C2) and (C3).

REFERENCES

1. El Wakil, M. M., Uyehara, O. A., and Myers, P. S.: A Theoretical Investigation of the Heating-Up Period of Injected Fuel Droplets Vaporizing in Air. NACA TN 3179, 1954.

2. Hughes, R. R., and Gilliland, E. R.: The Mechanics of Drops. Chem. Eng. Prog., vol. 48, no. 10, Oct. 1952, pp. 497-504.

3. Savic, P.: Hydrodynamical and Heat Transfer Problems of Liquid Spray Droplets. Feature Article, Quart. Bull., Gas Dynamics Div., Nat. Res. Council, Jan. 1 - Mar. 31, 1953.

4. Blanchard, Duncan C.: Experiments With Water Drops and the Interaction Between Them at Terminal Velocity in Air. Rep. No. RL-566, Project Cirrus, Contract No. W-36-039-SC-38141, Signal Corps, Office of Naval Res. and Gen. Elec. Res. Lab., July 30, 1951, pp. 102-130.

5. McDonald, James E.: Theoretical Cloud Physics Studies. Final Rep., Proj. No. NR 082093, Contract N-onr-757, Task Order (∞) Office of Naval Res. and Iowa State College, Jan. 31, 1953.

6. Conkie, W. R., and Savic, P.: Calculation of the Influence of Internal Circulation in a Liquid Drop on Heat Transfer and Drag. Rep. No. MT-23, Div. Mech. Eng., Nat. Res. Council, Oct. 22, 1953.

7. Maxwell, J. B.: Data Book on Hydrocarbons. D. Van Nostrand Co., Inc., 1950.

8. Timmermans, J.: Physico-Chemical Constants of Pure Organic Compounds. Elsevier Pub. Co., 1950.

9. Anon: Selected Values of Properties of Hydrocarbons, Res. Proj. 44, A.P.I. and Nat. Bur. Standards, July 1949.

10. Obert, E. W.: Elements of Thermodynamics and Heat Transfer. McGraw-Hill Book Co., Inc., 1949.

11. Hirschfelder, Joseph O., Curtiss, Charles F., and Bird, R. Byron: Molecular Theory of Gases and Liquids. John Wiley & Sons, Inc., 1954.

12. Ranz, W. E., and Marshall, W. R., Jr.: Evaporation From Drops. Chem. Eng. Prog., vol. 48, no. 3, Mar. 1952, pp. 141-146; no. 4, Apr. 1952, pp. 173-180.

13. Brikowski, H. J.: A Preliminary Experimental Investigation of Unsteady State Vaporization in Drops. Appendix I, M. S. Thesis, Univ. of Wis., 1954.

14. Gilliland, E. R.: Diffusion Coefficients in Gaseous Systems. Ind. and Eng. Chem., vol. 26, no. 6, June 1934, pp. 681-685.

15. Ingebo, Robert D.: Vaporization Rates and Heat-Transfer Coefficients for Pure Liquid Drops. NACA TN 2368, 1951.

16. Hougen, Olaf A., and Watson, Kenneth M.: Chemical Process Principles. John Wiley & Sons, Inc., 1947, p. 977.

17. Schlichting, Hermann: Grenzschicht-Theorie. G. Braun (Karlsruhe), 1951.

18. Buckingham, E.: On Physically Simular Systems: Illustrations of the Use of Dimensional Equations. Phys. Rev., vol. 4, no. 4, Oct. 1914, pp. 345-376.

19. Ackermann, G.: Wärmeübergang und molekulare Stoffübertragung im gleichen Feld bei grossen Temperatur- und Partialdruckdifferenzen. Forschungsheft 382, Forsch. Geb. Ing.-Wes., 1937.

20. McAdams, William H.: Heat Transmission. Second ed., McGraw-Hill Book Co., Inc., 1942.

TABLE I

CONDITIONS FOR EXPERIMENTS

Fuels	Air temperatures, °F	Drop radius, in.	Air velocity, in./sec
n-Hexane	200 to 620	0.030 to 0.040	70 to 100
n-Heptane	175 to 620	.031 to 0.041	70 to 100
n-Octane	125 to 620	.032 to 0.041	50 to 300
Isooctane	200 to 620	.030 to 0.040	70 to 100
n-Nonane	200 to 620	.032 to 0.042	70 to 100
n-Decane	200 to 620	.032 to 0.042	70 to 100
Cetane	125 to 225	.033 to 0.042	50 to 300

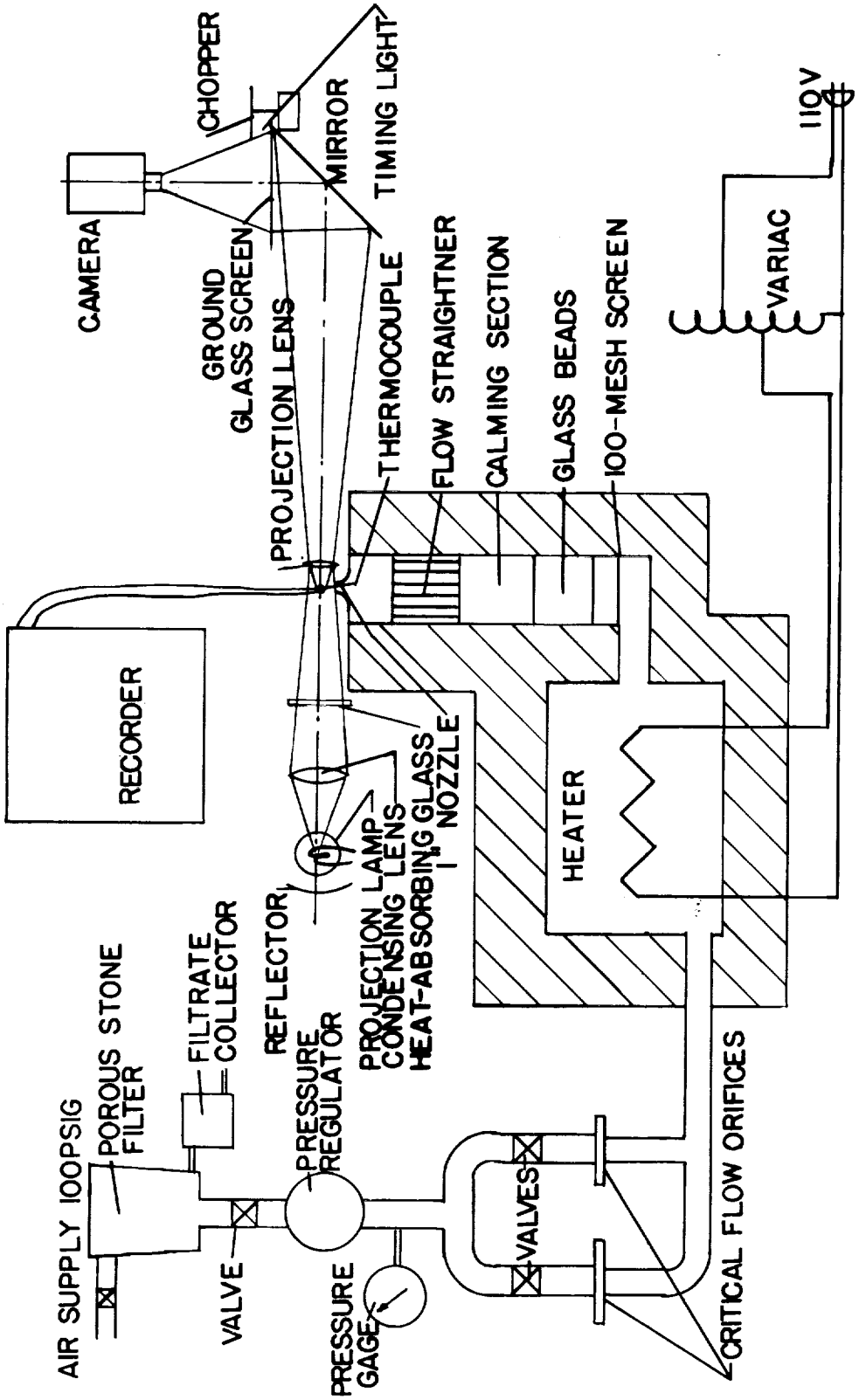

Figure 1.- Schematic diagram of experimental apparatus.

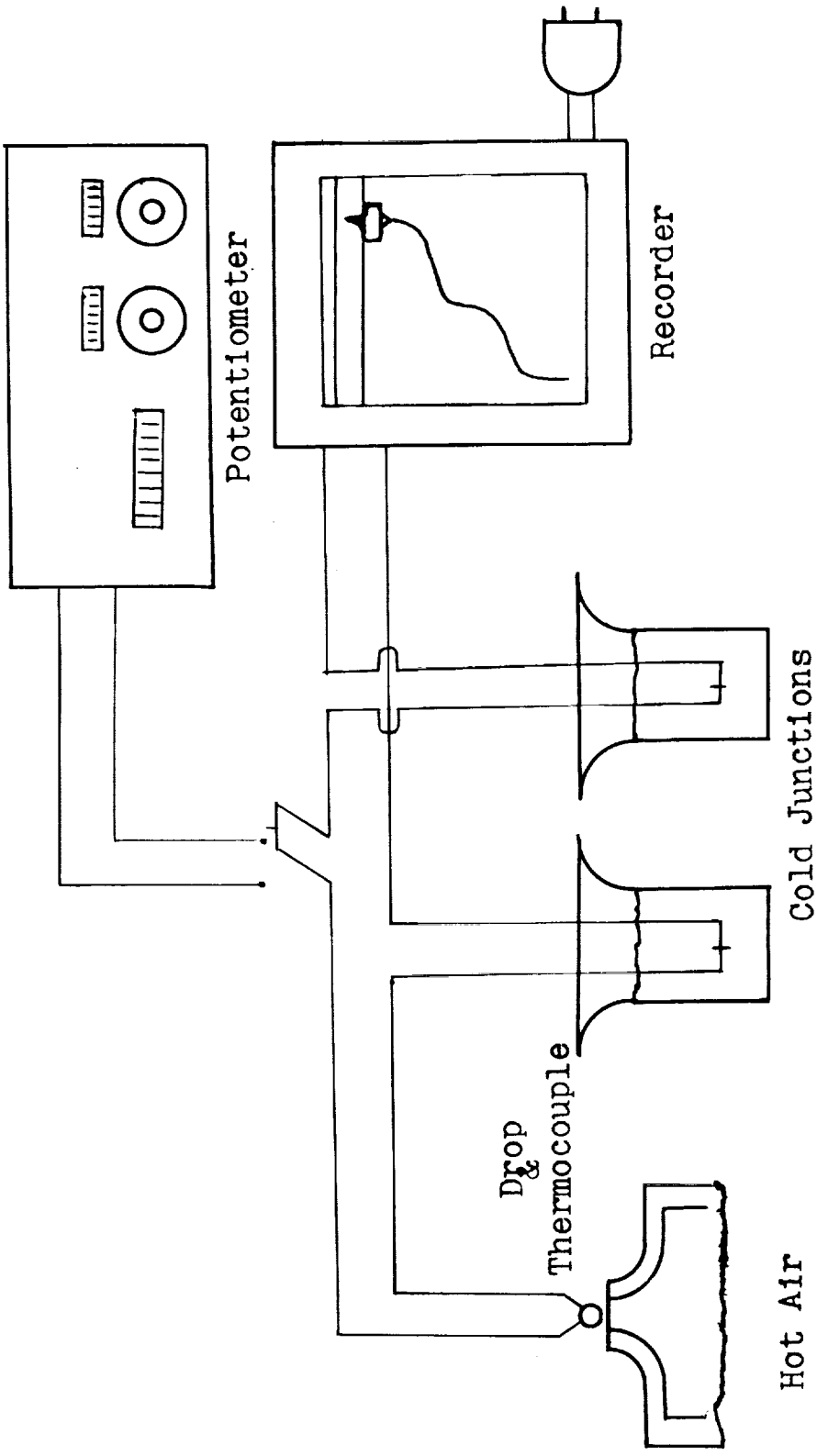

Figure 2.- Schematic diagram of temperature-recording system.

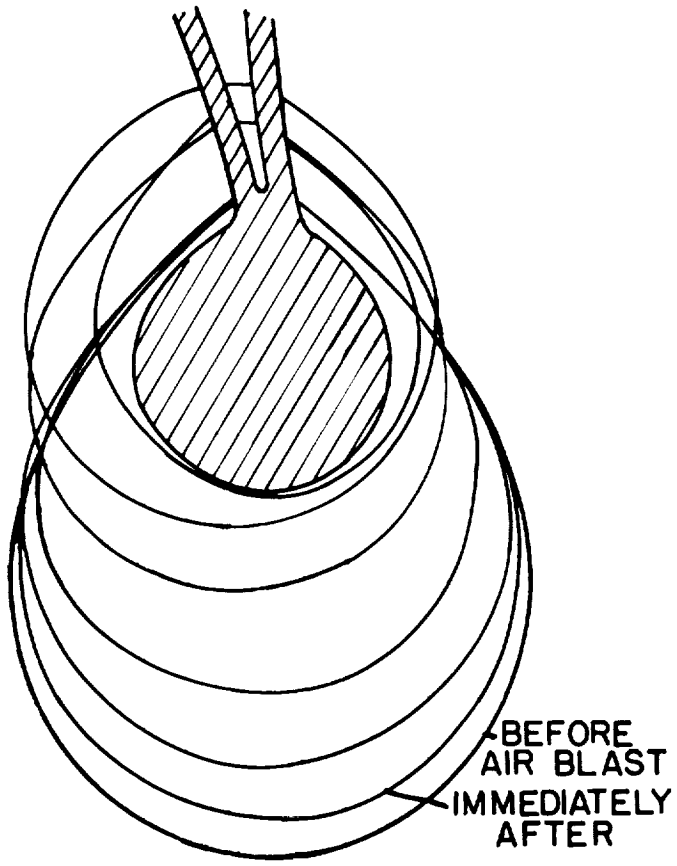

Figure 3.- Experimental drop shapes.

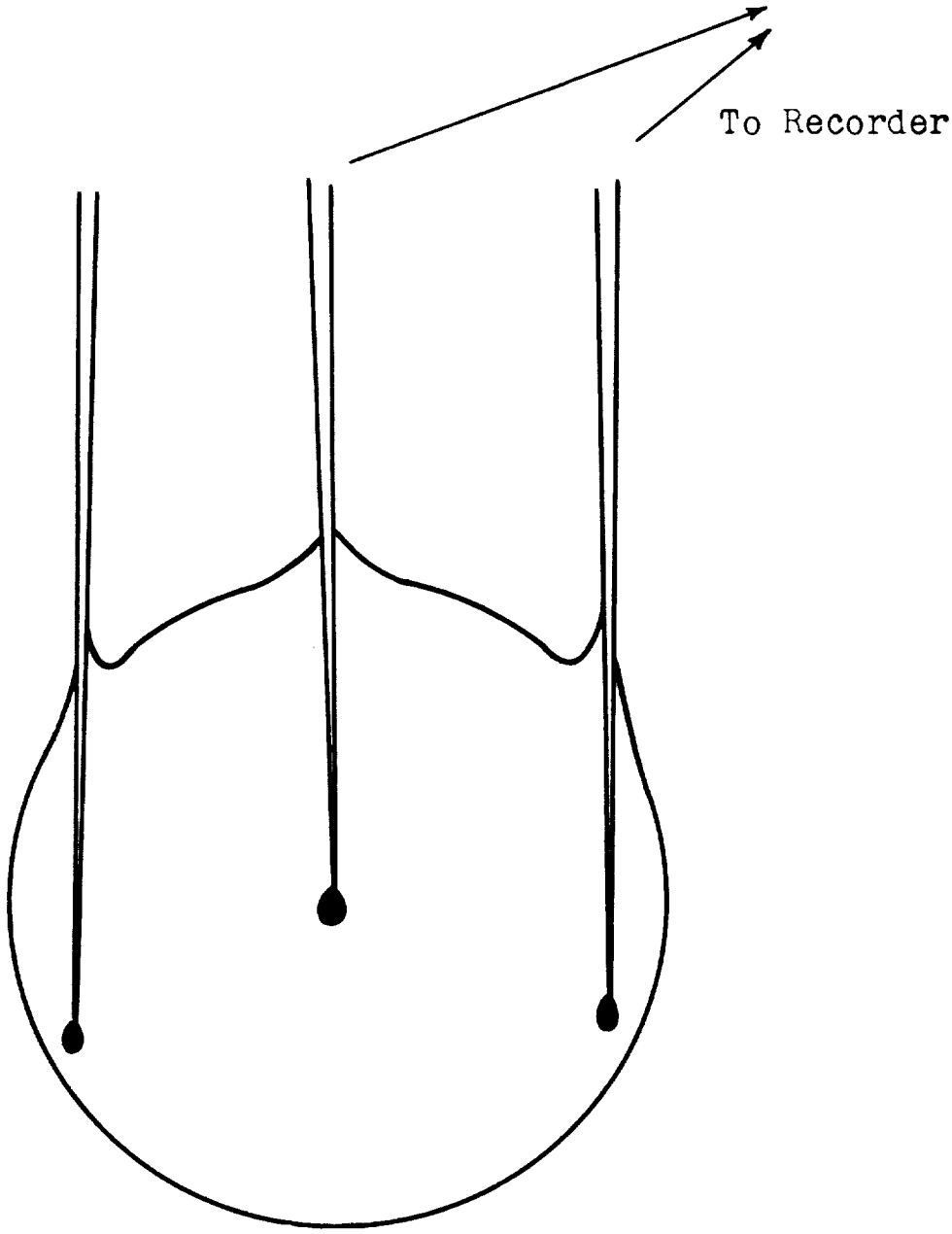

Figure 4.- Drop hanging on three thermocouples.

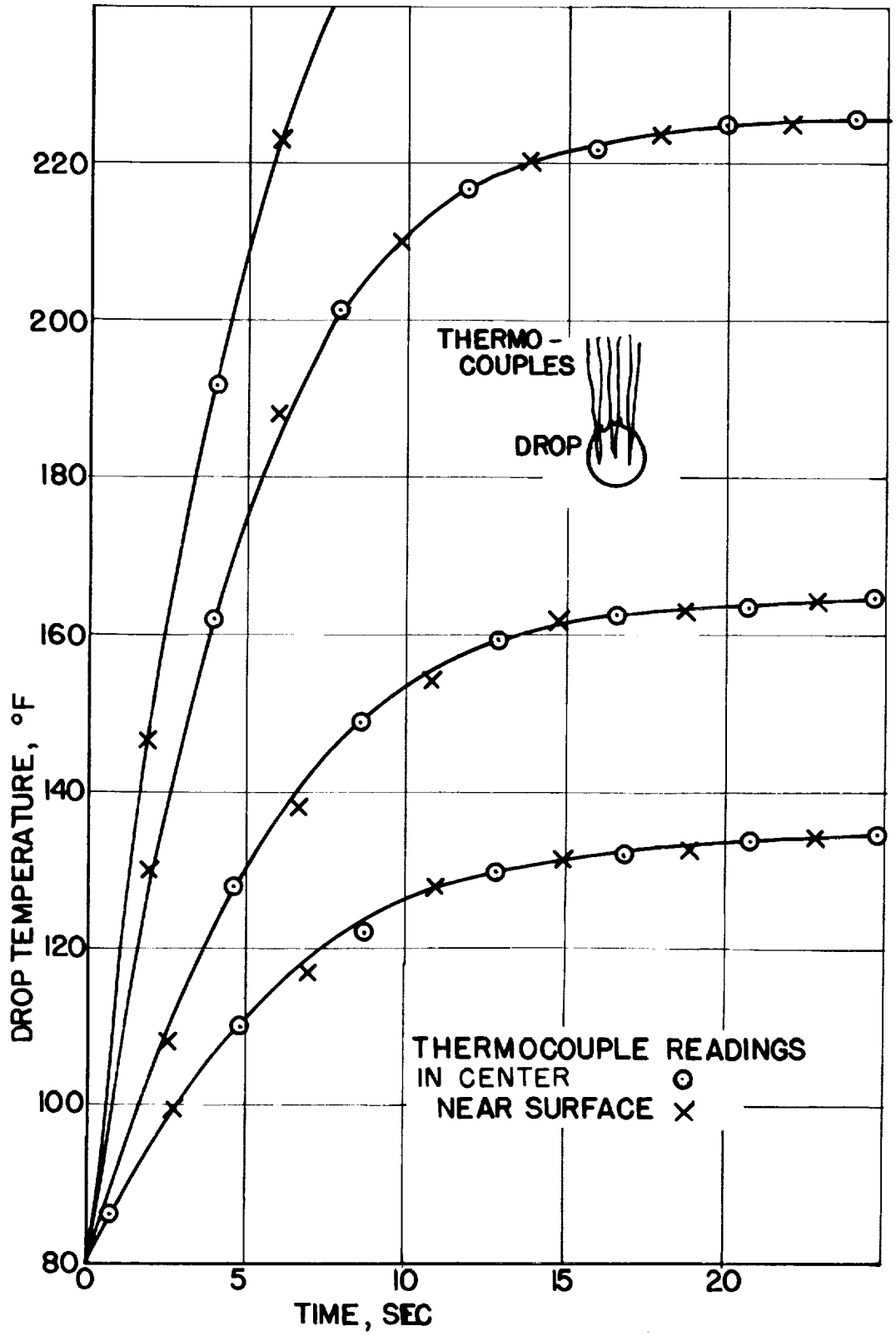

Figure 5.- Temperature-time histories of center and surface temperatures of cetane droplets.

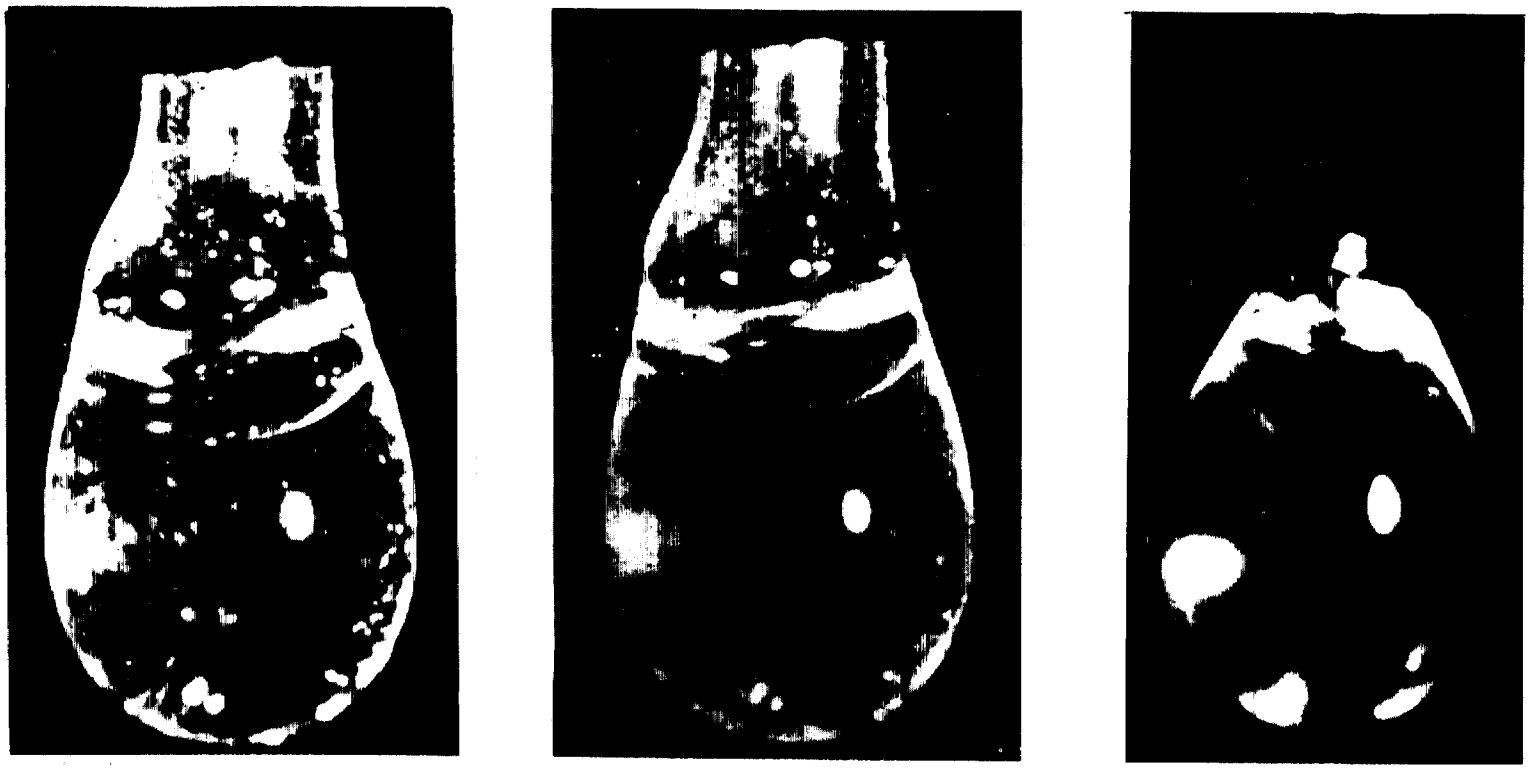

(a) n-Octane in still air; 64 frames per second.

(b) n-Octane in still air; 16 frames per second.

(c) Cetane in an air stream; 64 frames per second.

L-89338

Figure 6.- Aluminum oxide particles showing circulation inside drops.

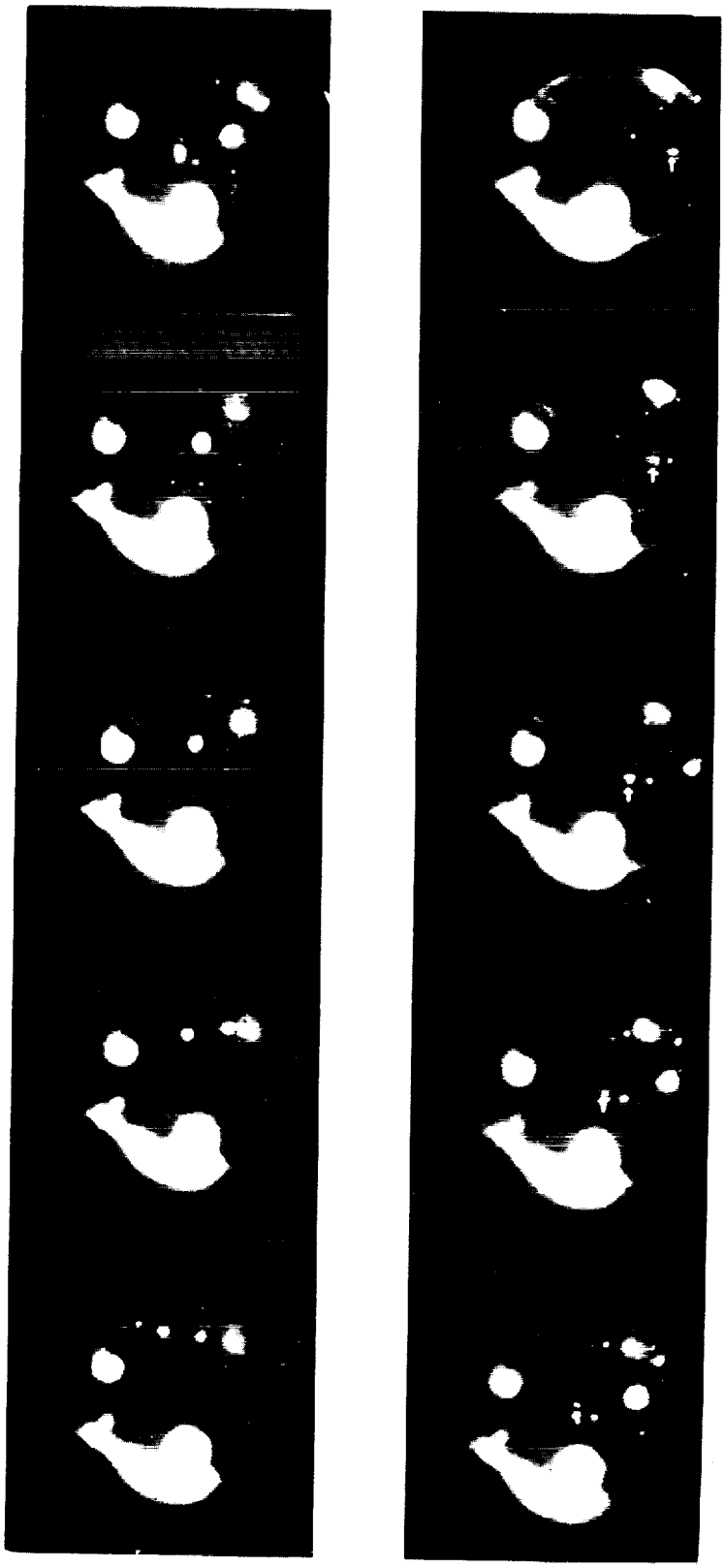

L-89339

Figure 7.- High-speed photographs of internal circulation in drops. Cetane drop in 6-foot-per-second upward air stream; frames 0.005 second apart.

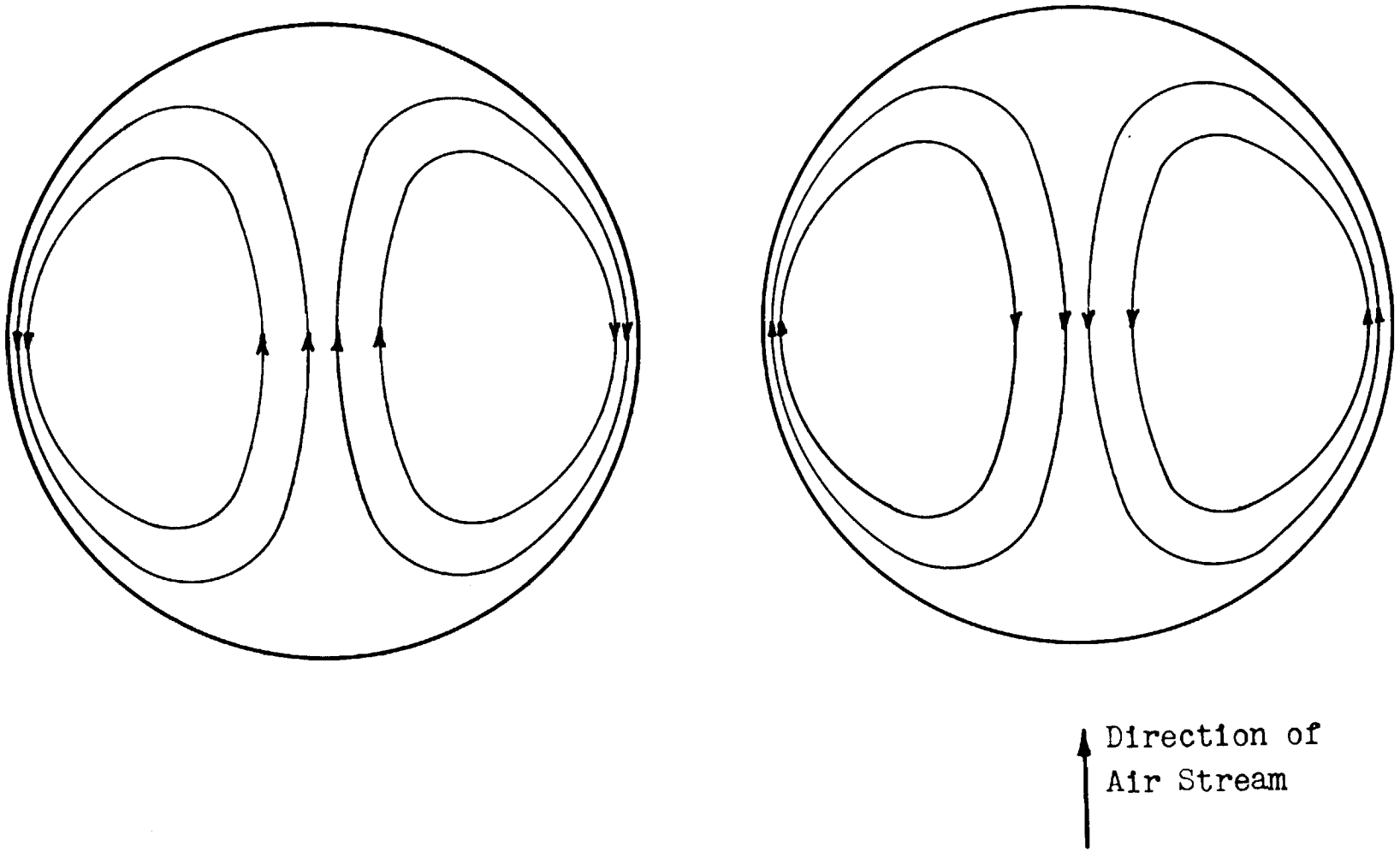

(a) In still air.

(b) In an air stream.

Figure 8.- Circulation in drops.

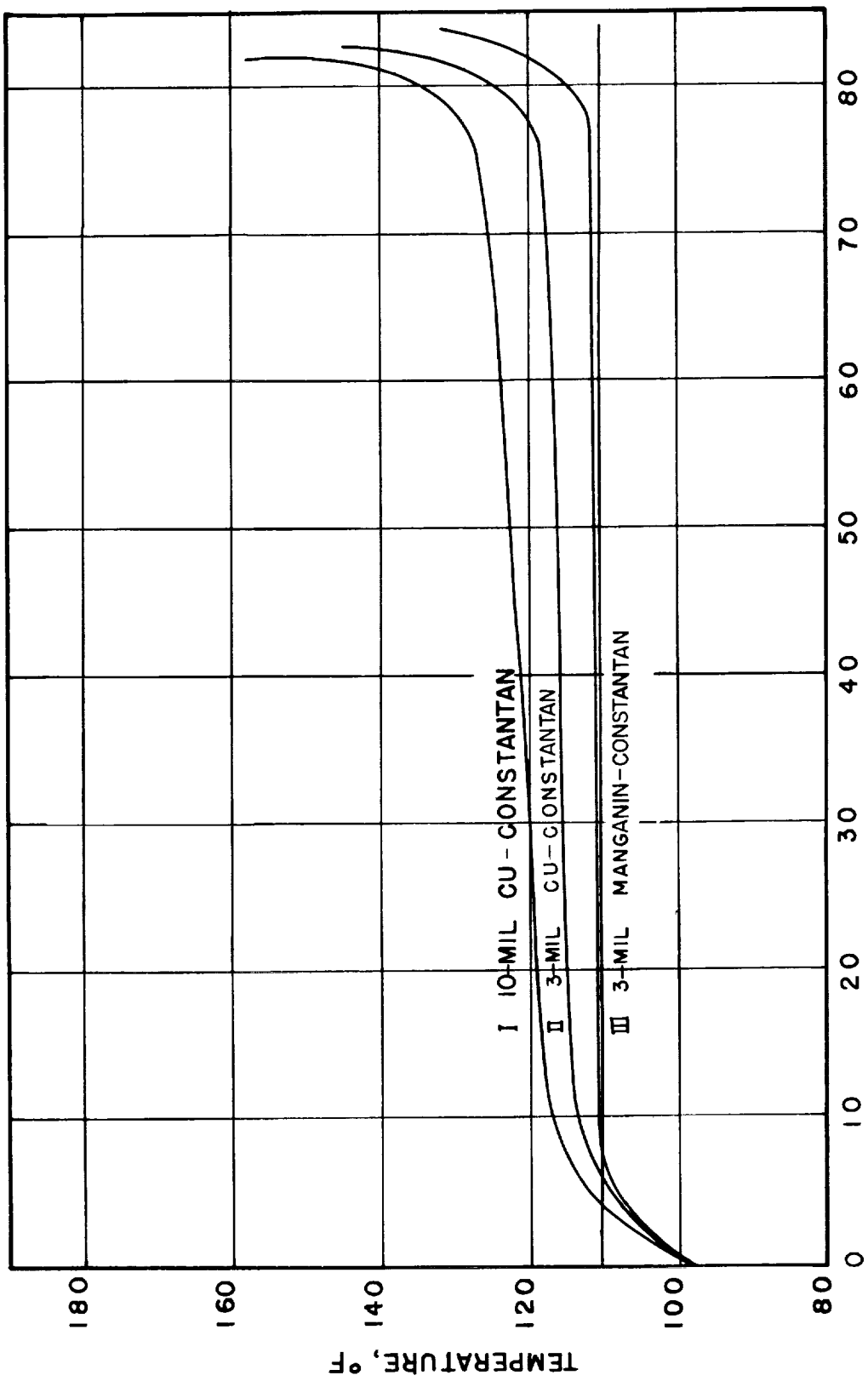

Figure 9.- Experimental time-temperature curves using water on different thermocouples in 300° F air blast.

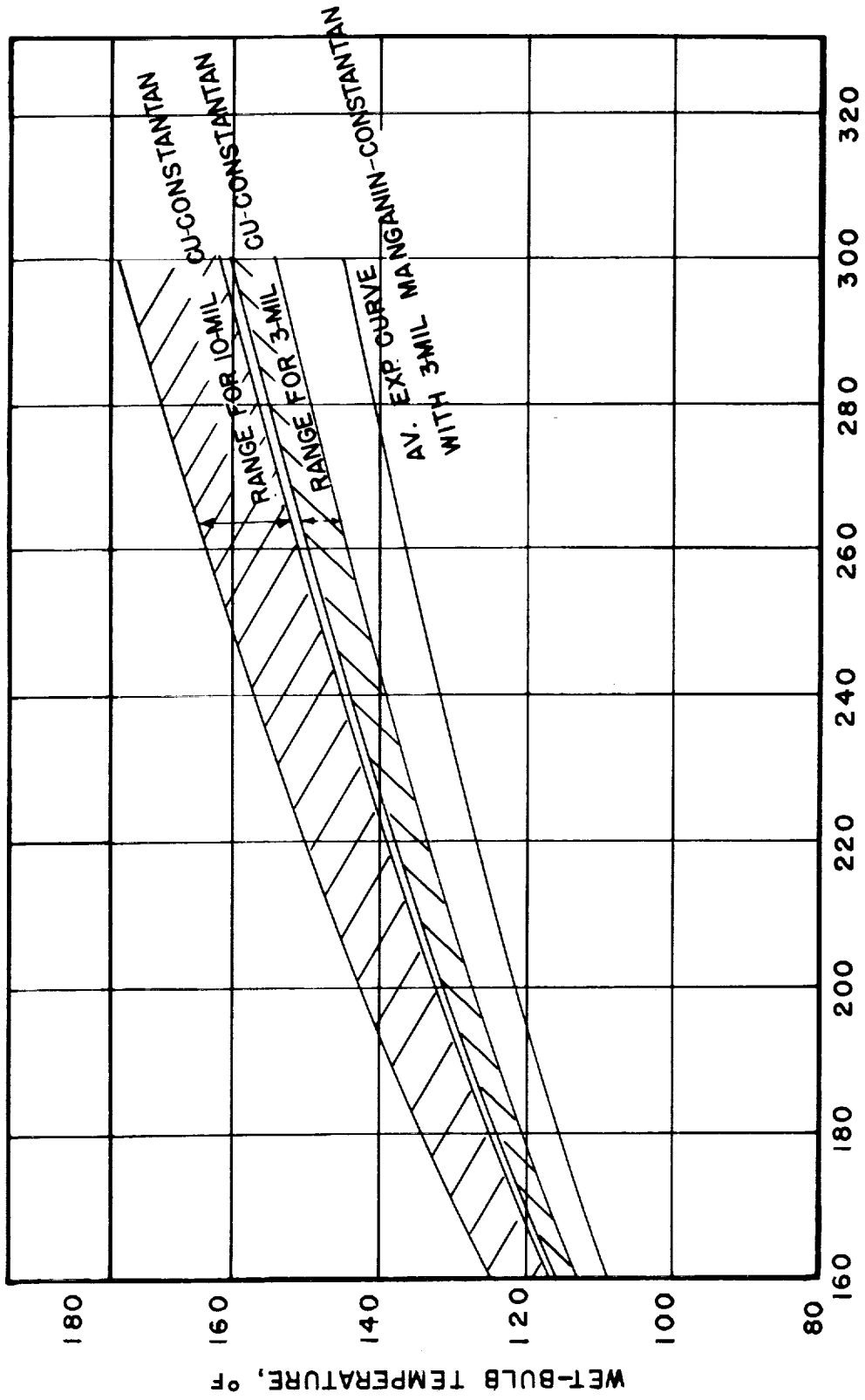

Figure 10.- Experimental wet-bulb temperatures for n-octane using different thermocouples and air temperatures.

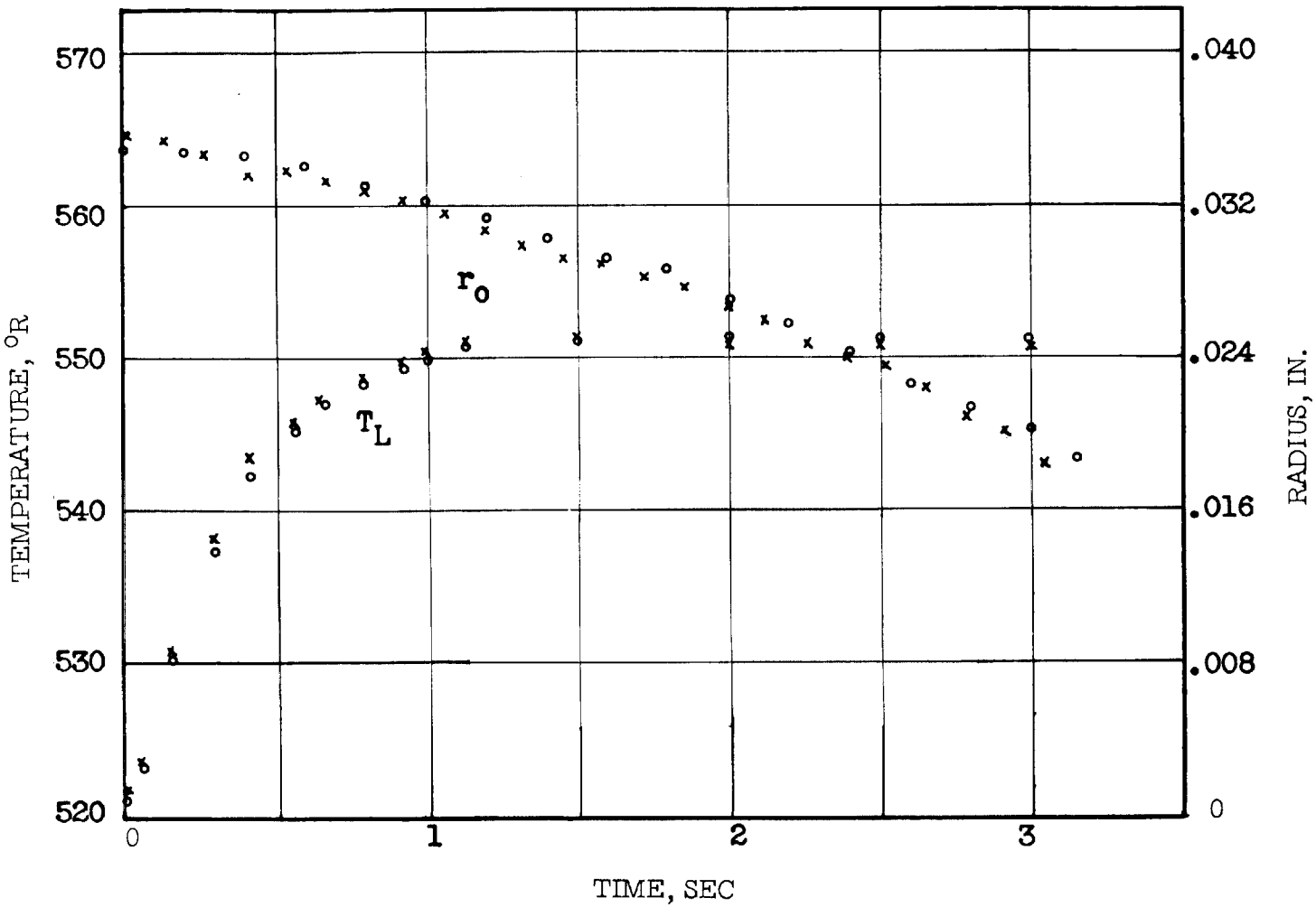

(a) n-Hexane. Air temperature, 1,073° R; air velocity, 93 inches per second.

Figure 11.- Experimental reproducibility.

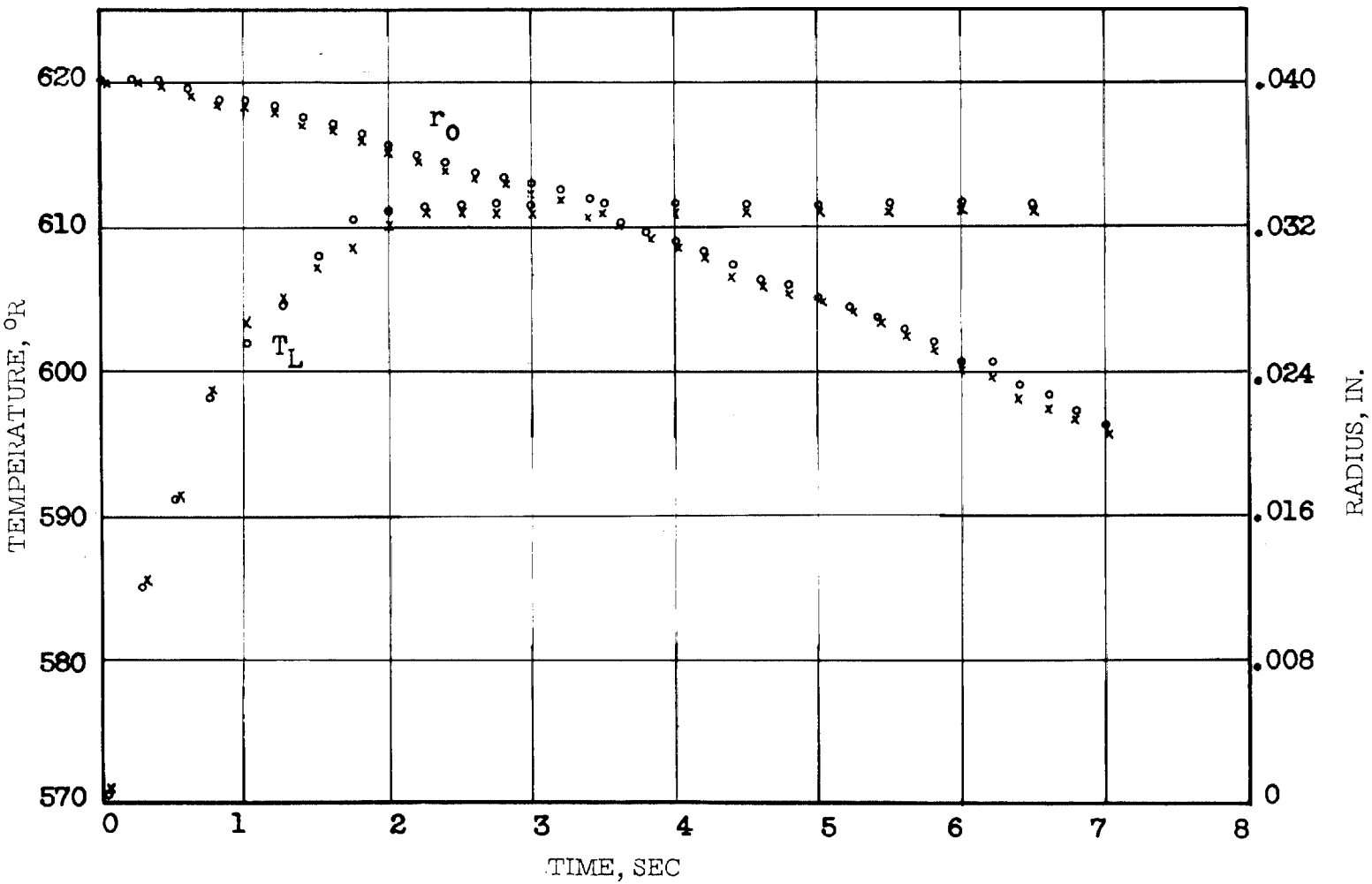

(b) n-Heptane. Air temperature, 812° R; air velocity, 92.6 inches per second.

Figure 11.- Concluded.

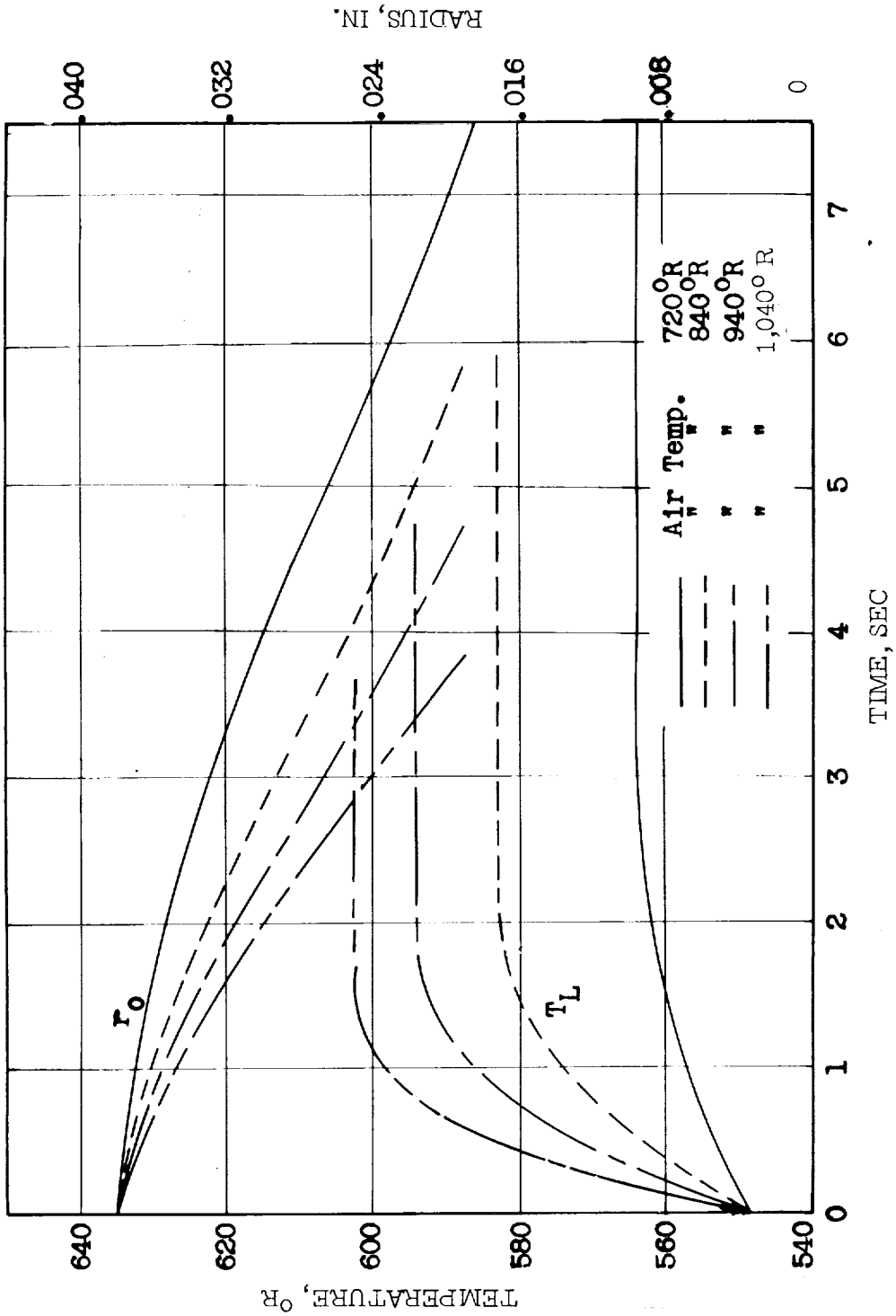

(a) Isooctane drops.

Figure 12.- Experimental temperature-time and radius-time histories at different air temperatures. Air velocity, 84 to 94 inches per second.

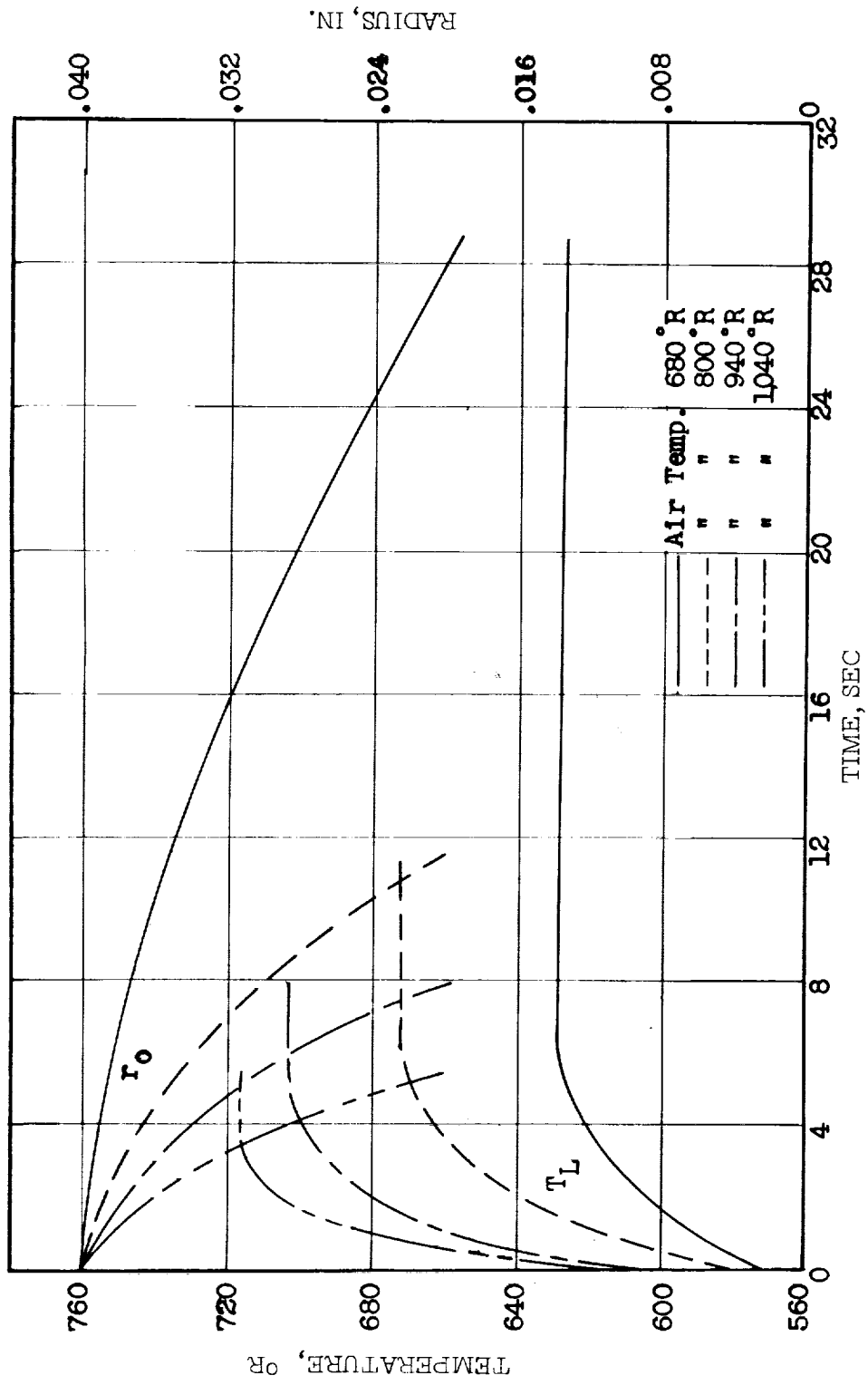

(b) n-Decane drops.

Figure 12.- Concluded.

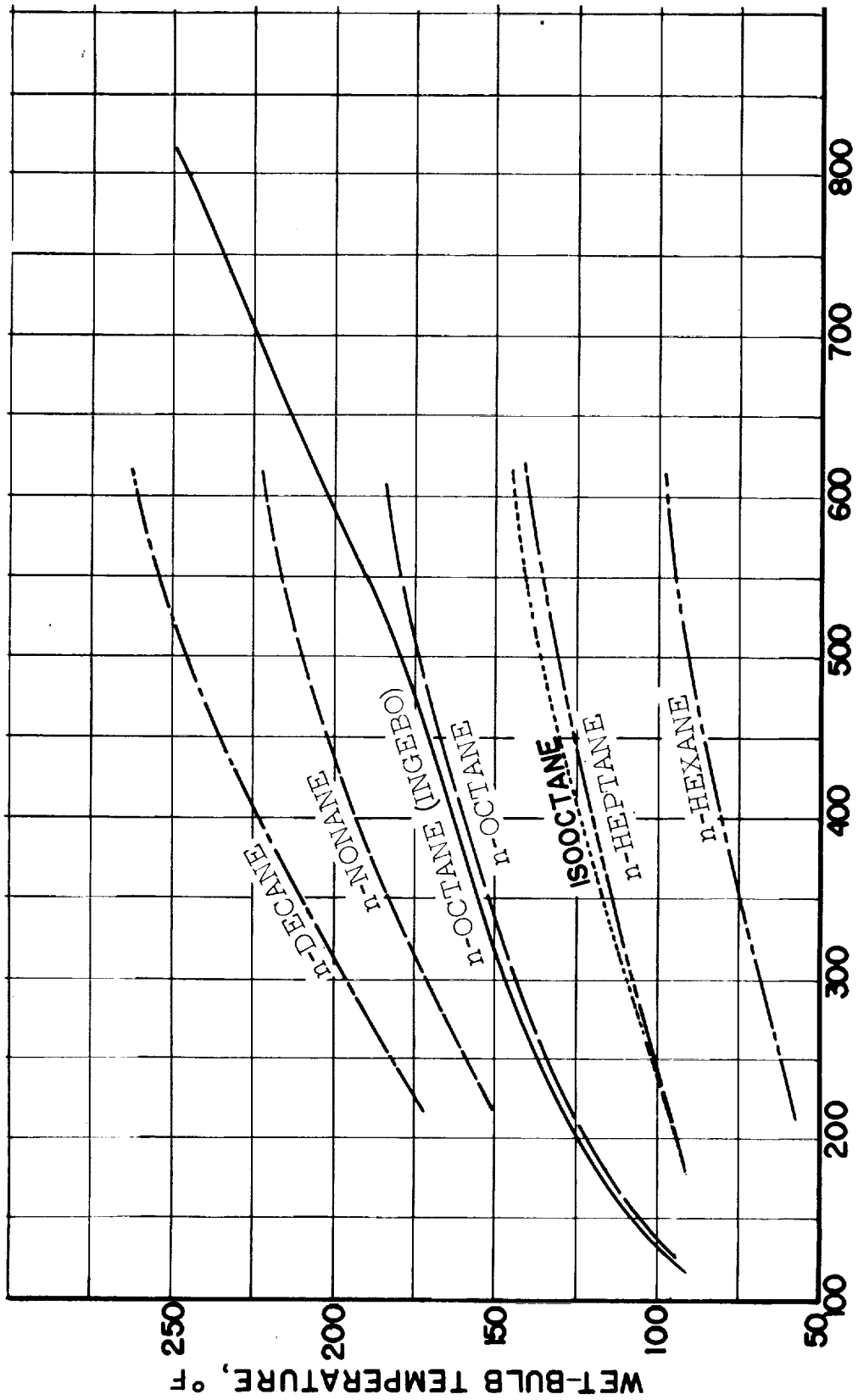

Figure 13.- Wet-bulb temperatures for given fuels.

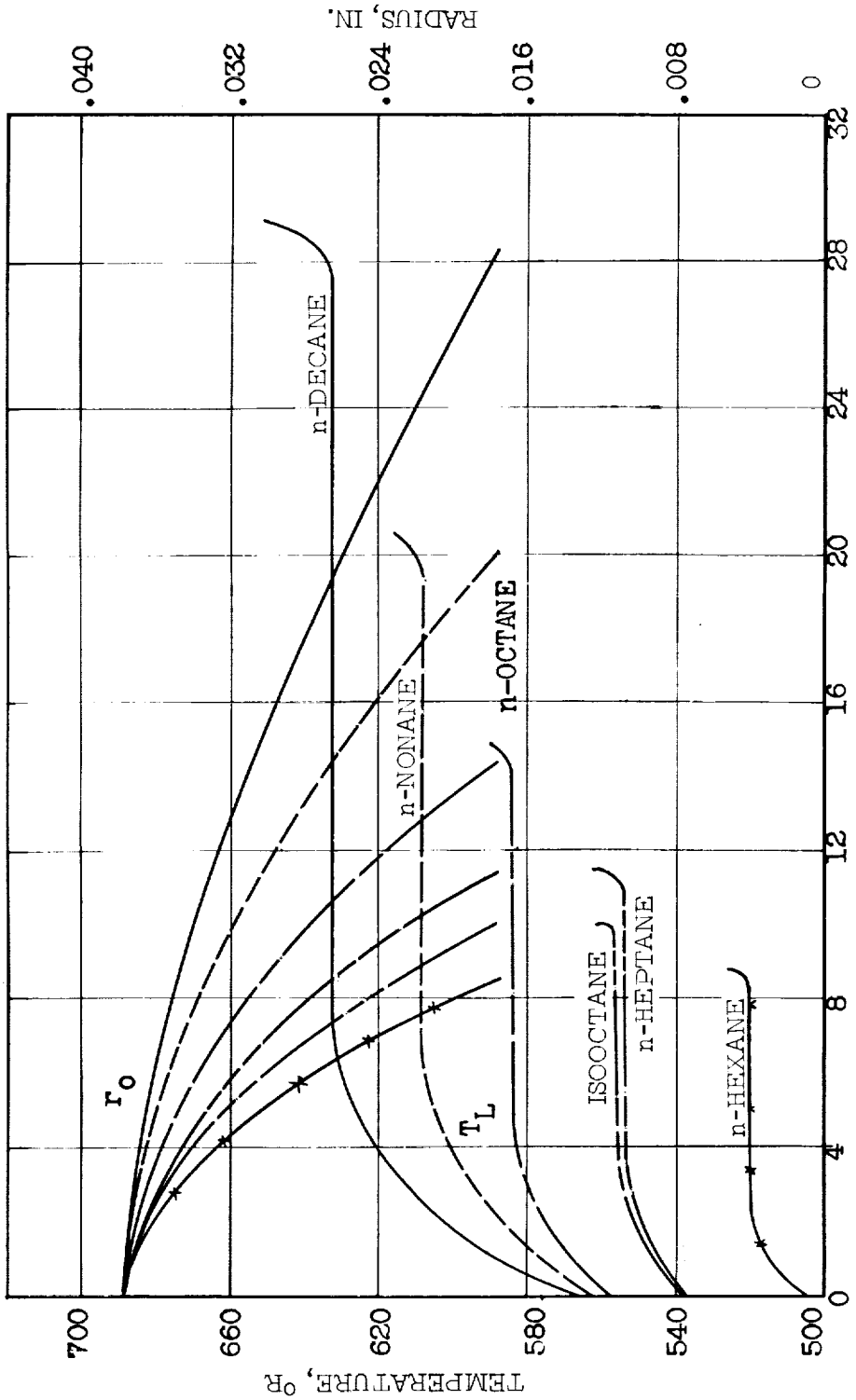

(a) Air temperature, 680° R.

Figure 14.- Experimental temperature-time and radius-time histories of droplets of different compositions. Air velocity, 90 inches per second.

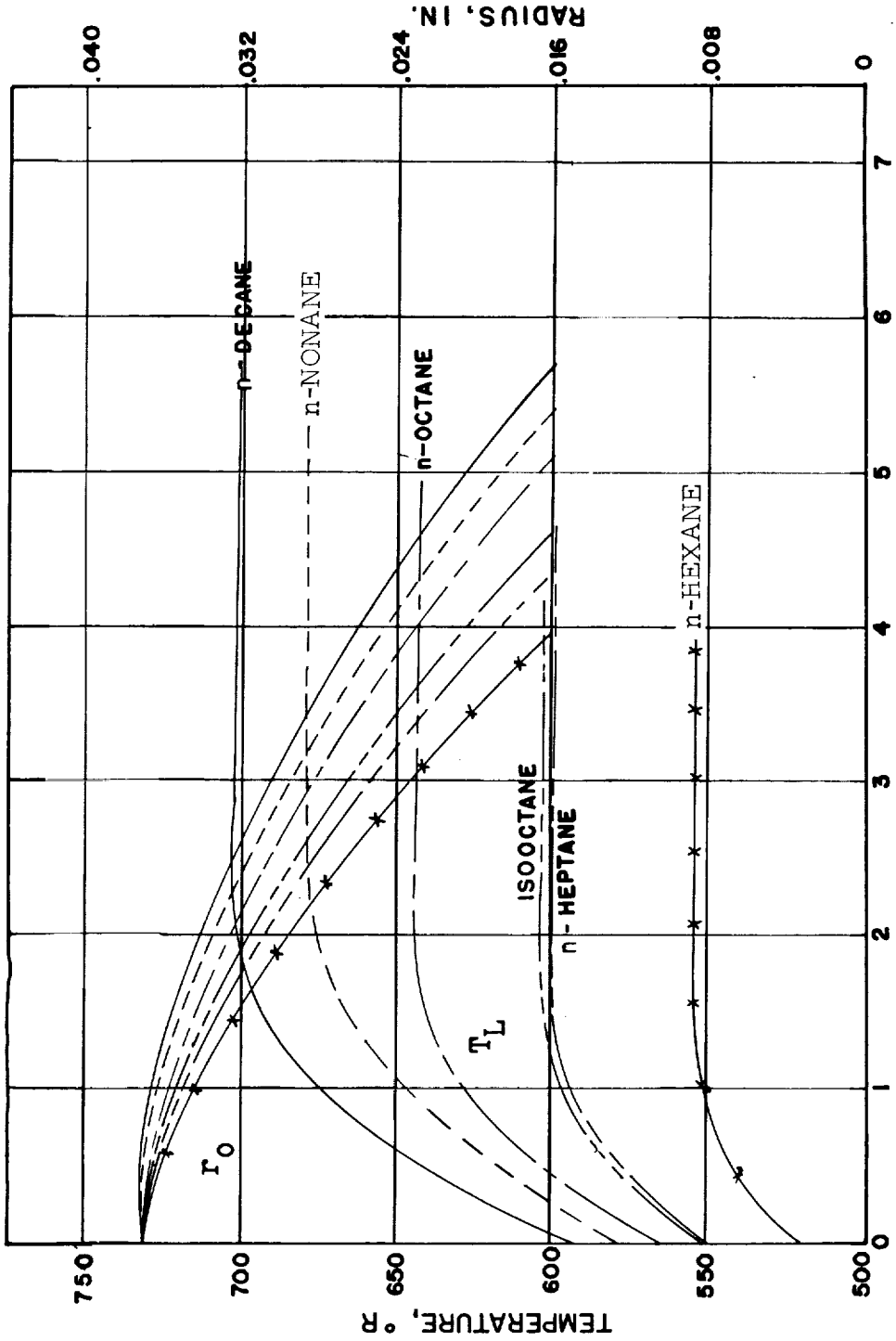

(b) Air temperature, 1,000° R.

Figure 14.- Concluded.

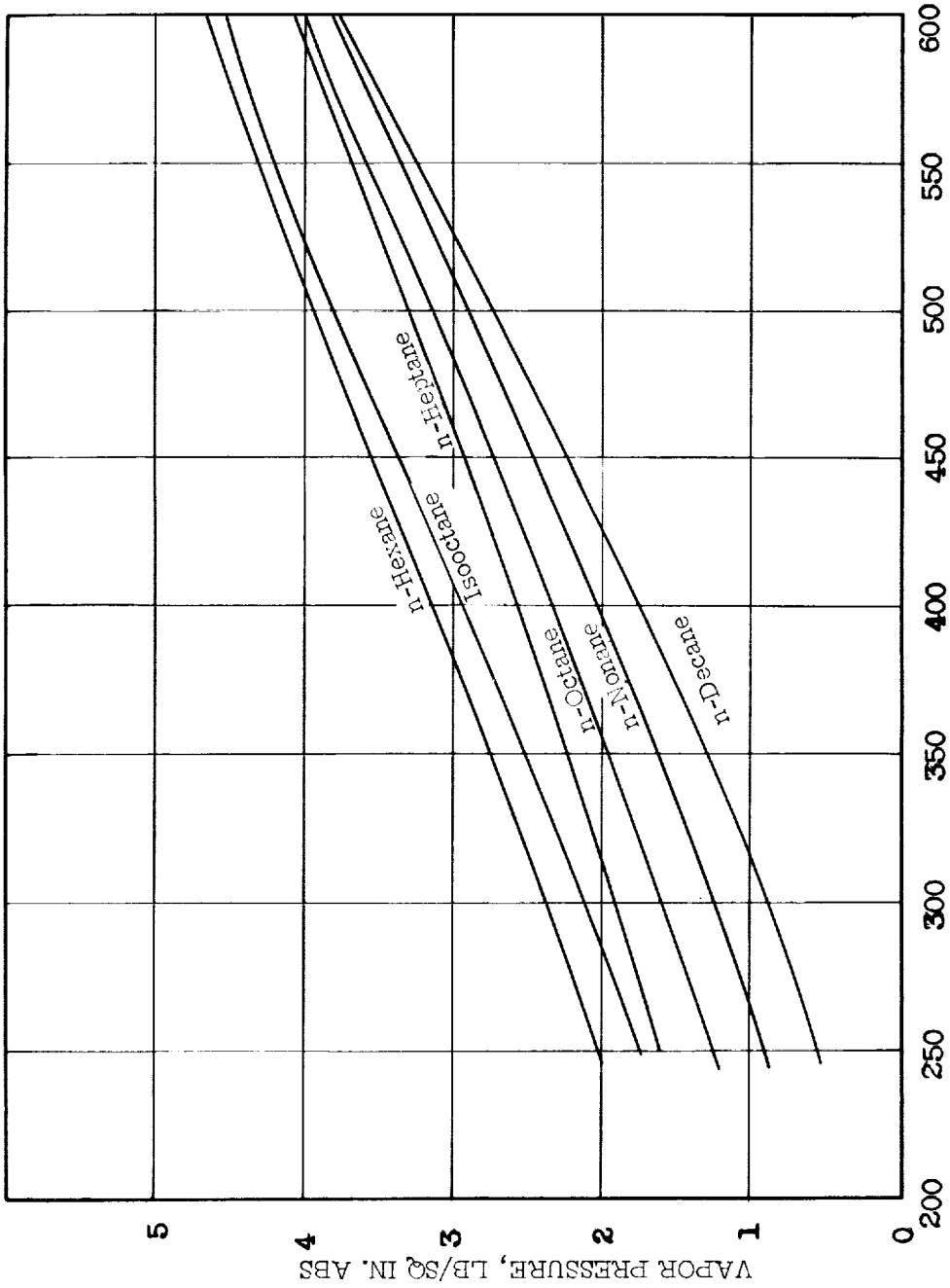

Figure 15.- Vapor pressure at wet-bulb temperature against air temperature.

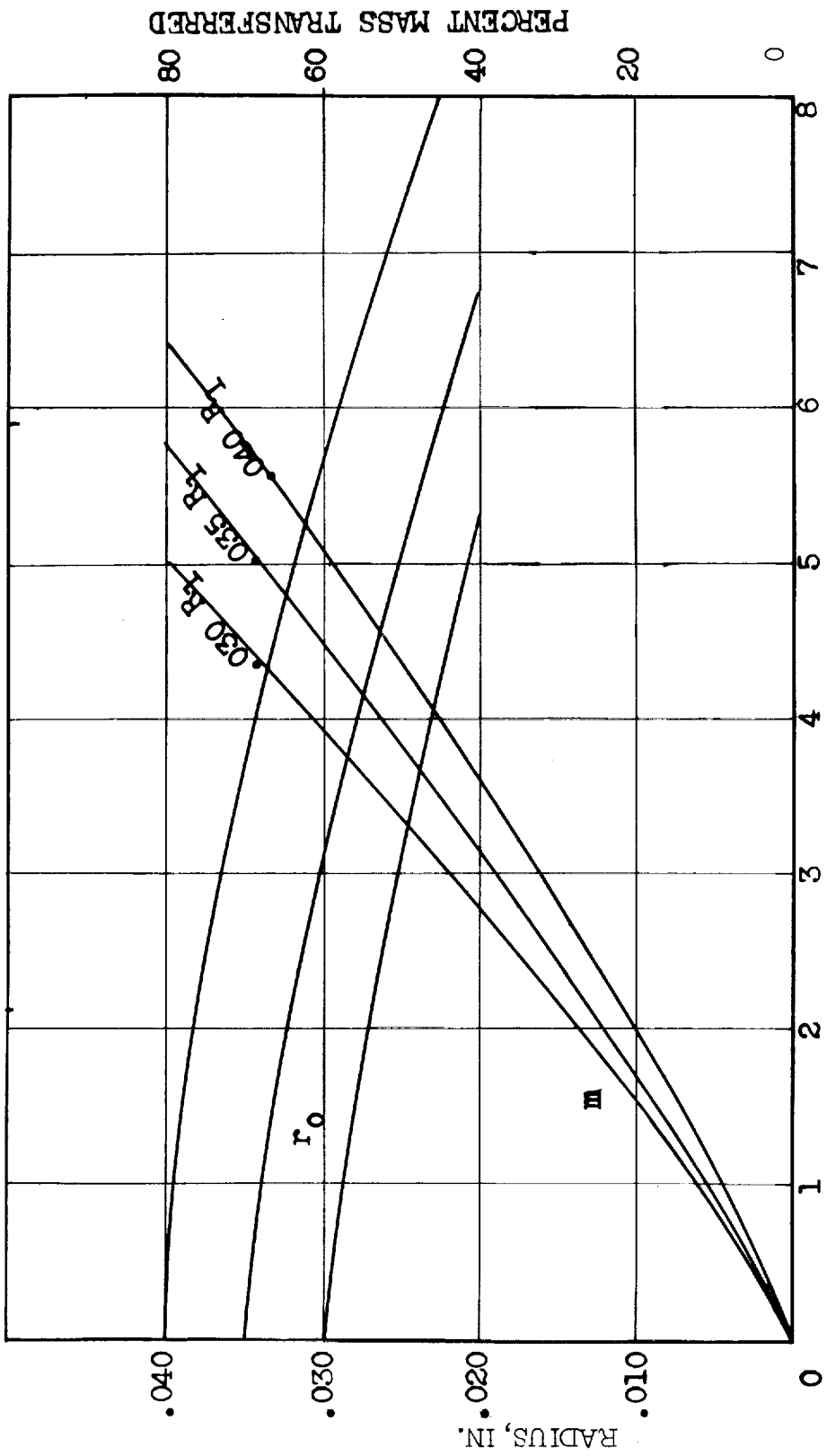

(a) n-Hexane.

Figure 16.- Experimental droplet histories with different initial radii. Air temperature, 680° R; air velocity, 90 inches per second.

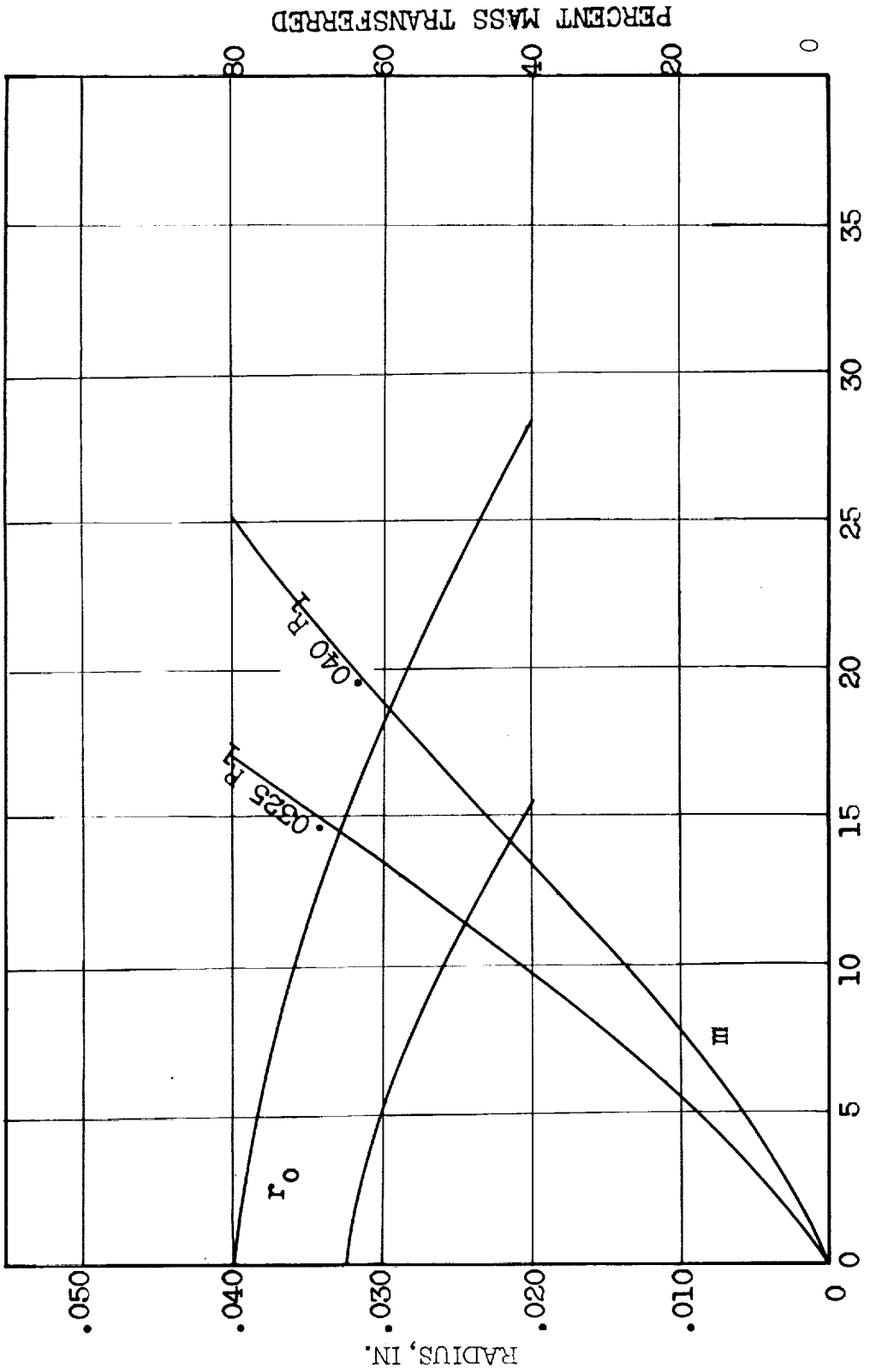

(b) n-Decane.

Figure 16.- Concluded.

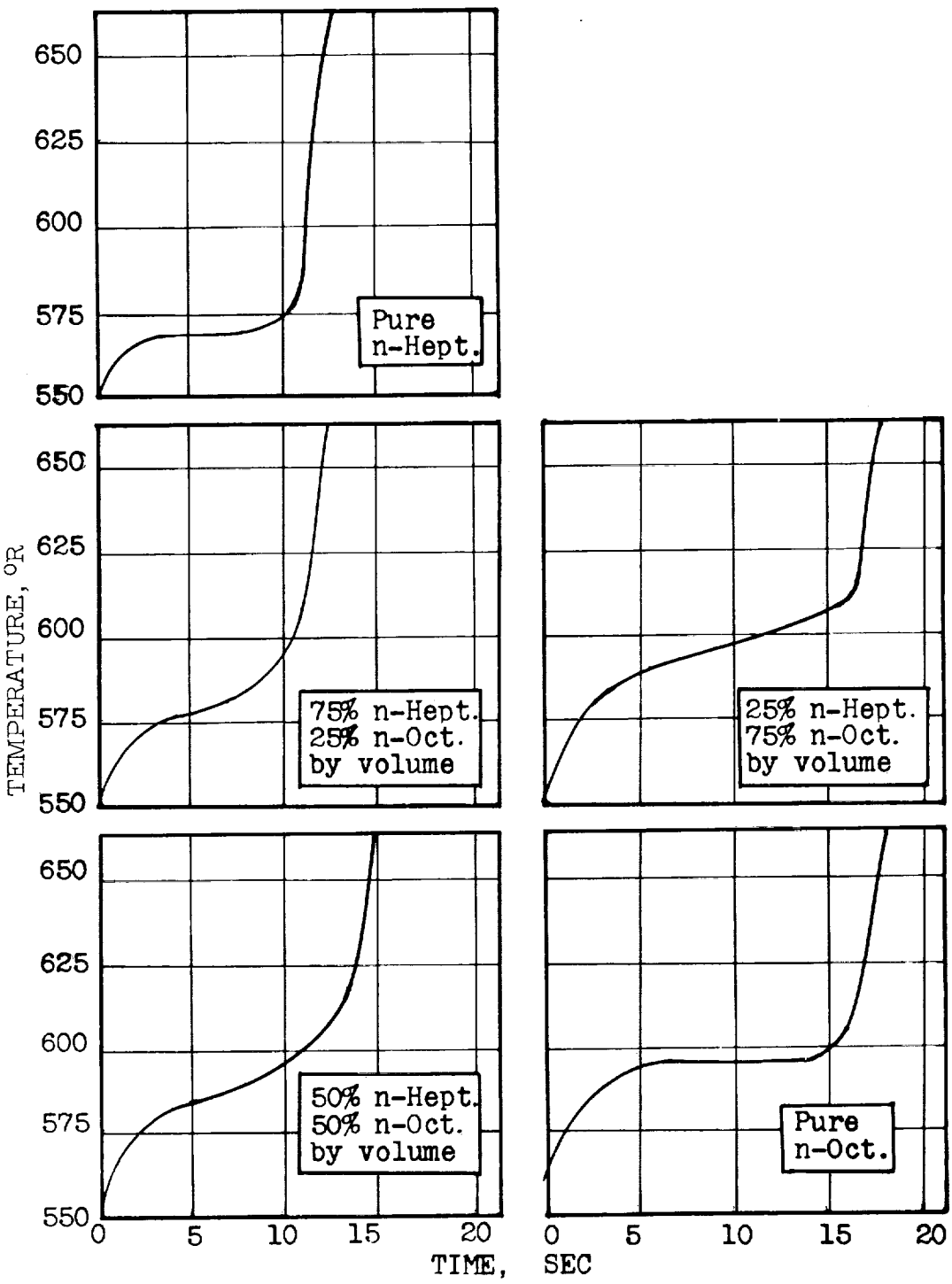

(a) Mixtures of n-heptane and n-octane. Average air temperature, 700° R.

Figure 17.- Temperature-time histories. Average air velocity, 90 inches per second; average drop size, 0.035 inch.

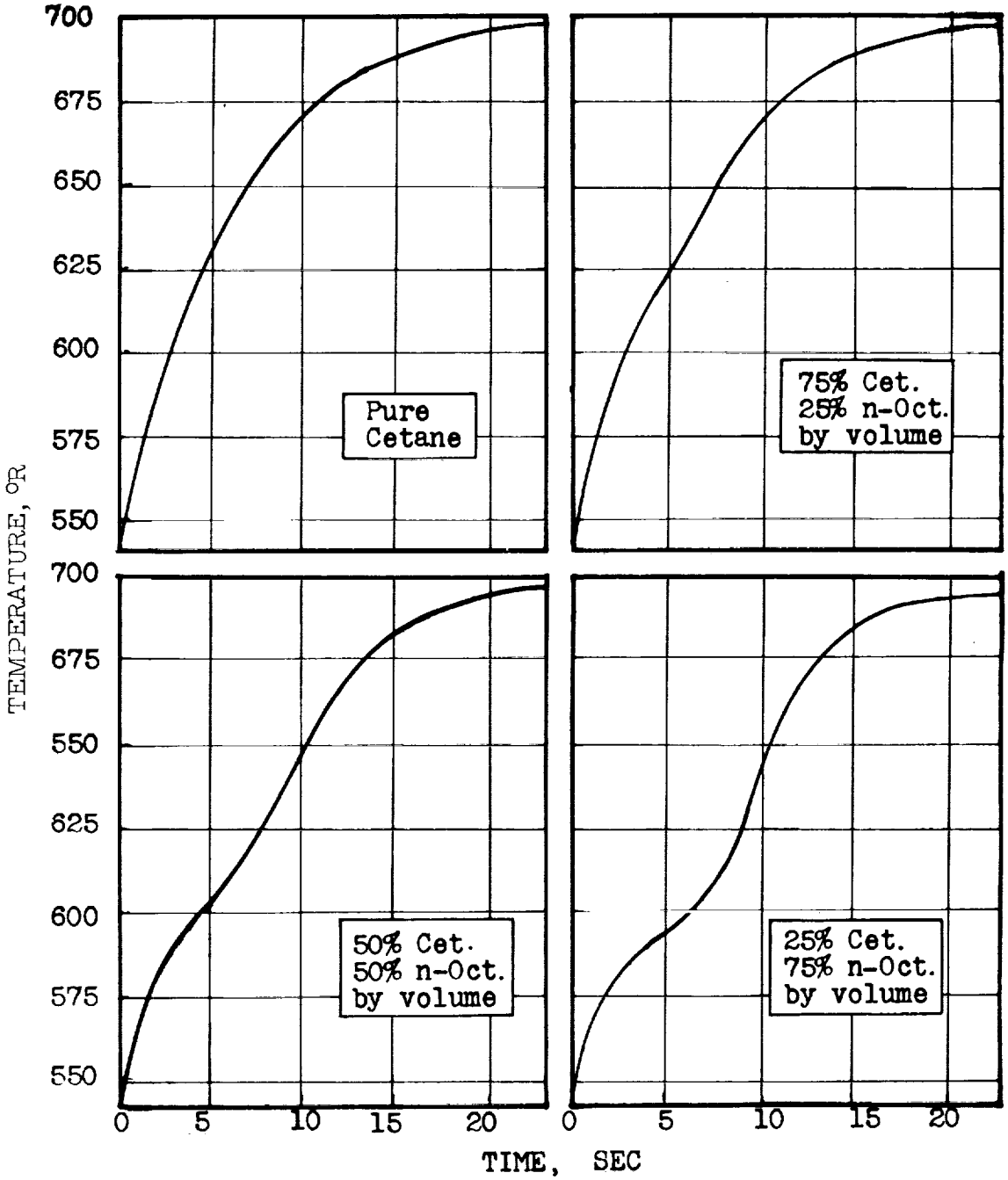

(b) Mixtures of n-octane and cetane. Average air temperature, 710° R.

Figure 17.- Concluded.

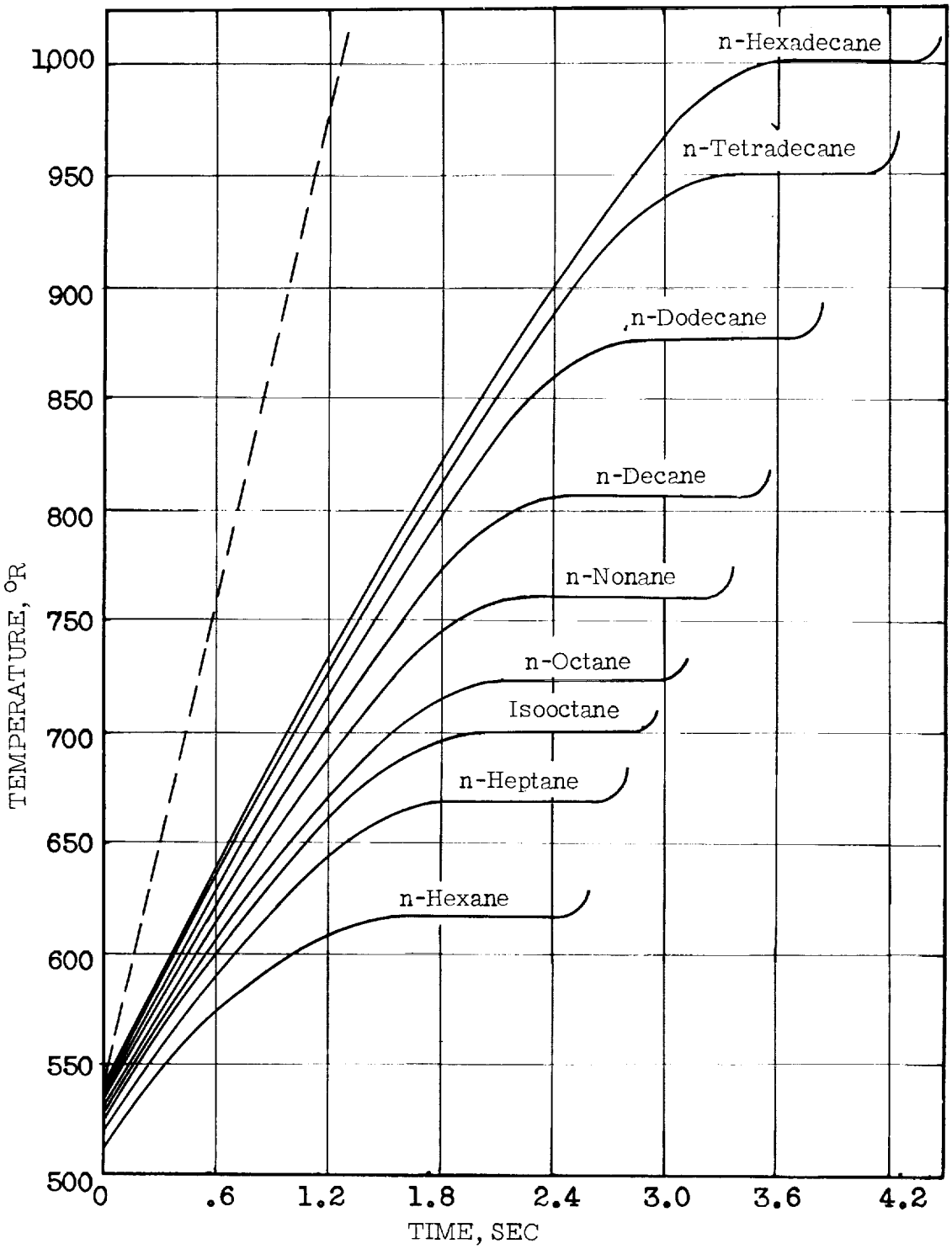

Figure 18.- Temperature-time histories of burning drops. Air temperature, 2,000° R.

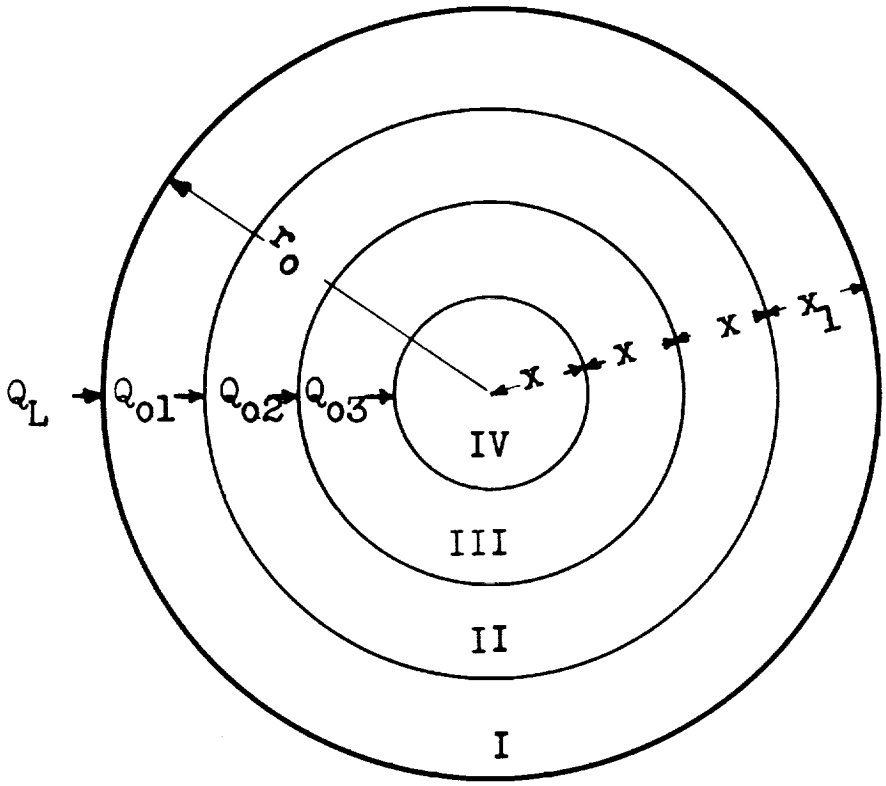

Figure 19.- Heat transfer into droplet with finite thermal conductivity.

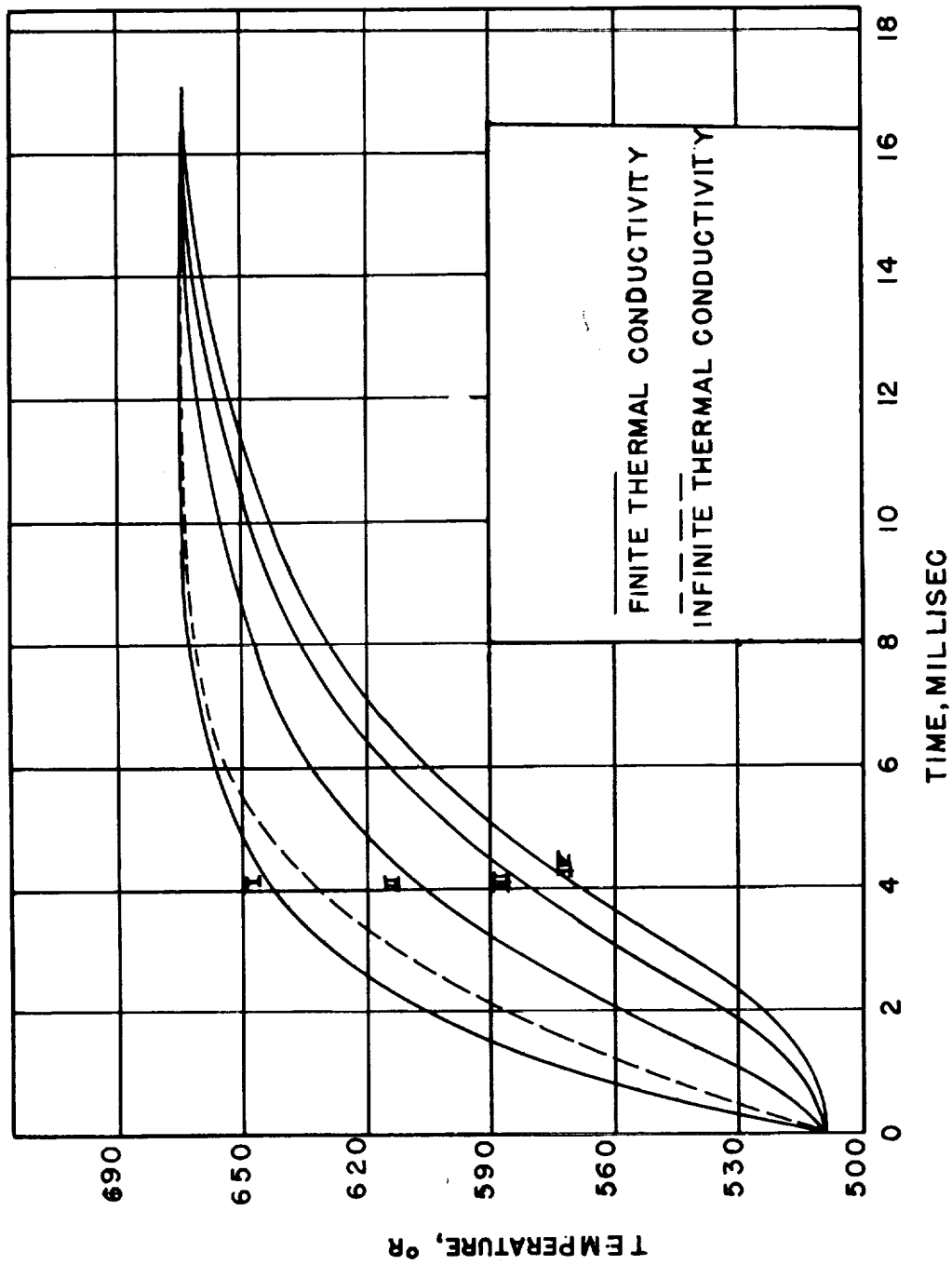

Figure 20.- Calculated temperature-time histories of n-octane droplet using finite and infinite thermal conductivity. Roman numerals are from figure 19; $T_B = 960^\circ$ R; $r_{o1} = 50$ microns; $U_1 = 1,200$ inches per second.

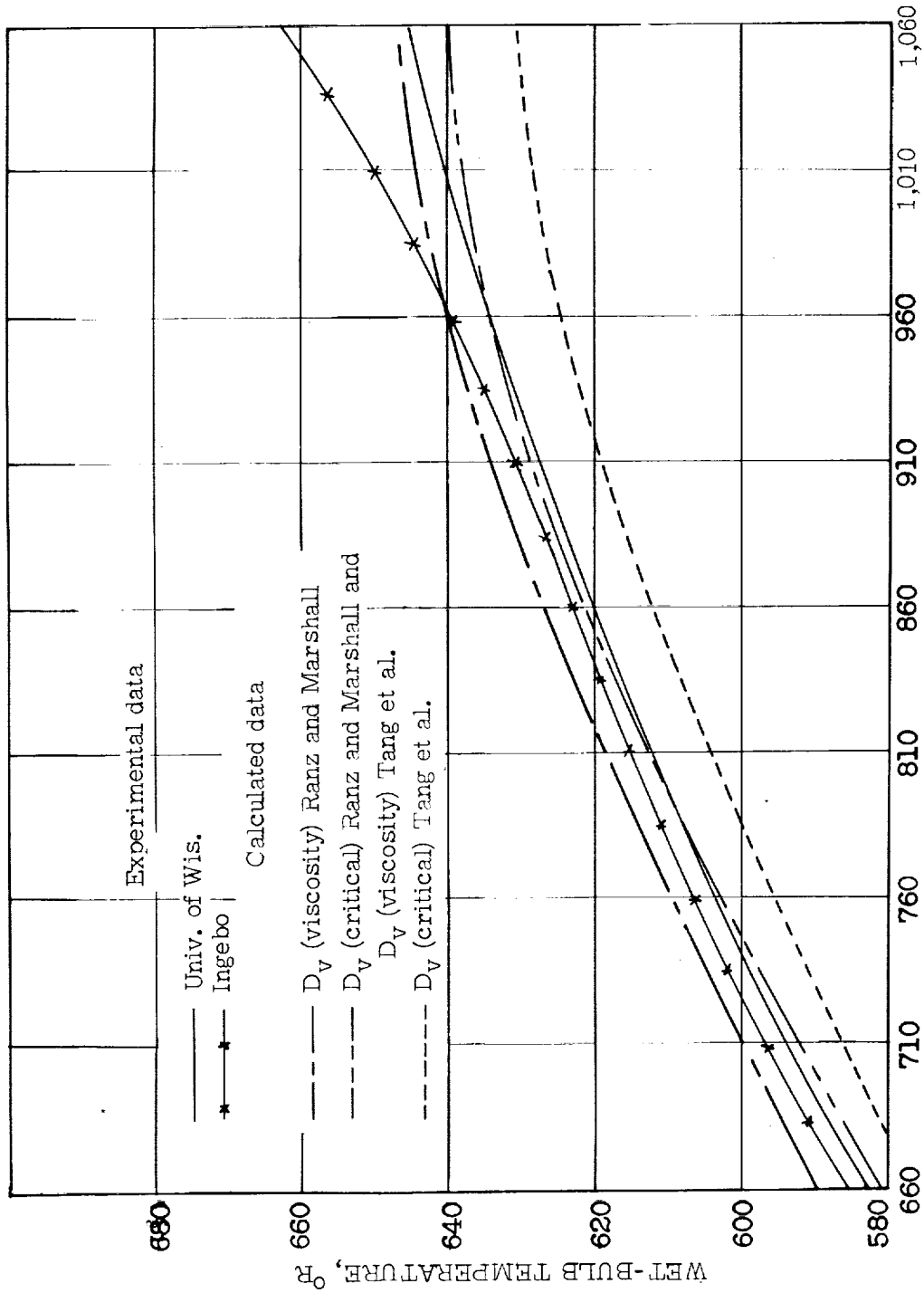

Figure 21.- Experimental and calculated wet-bulb temperatures of n-octane for different air temperatures.

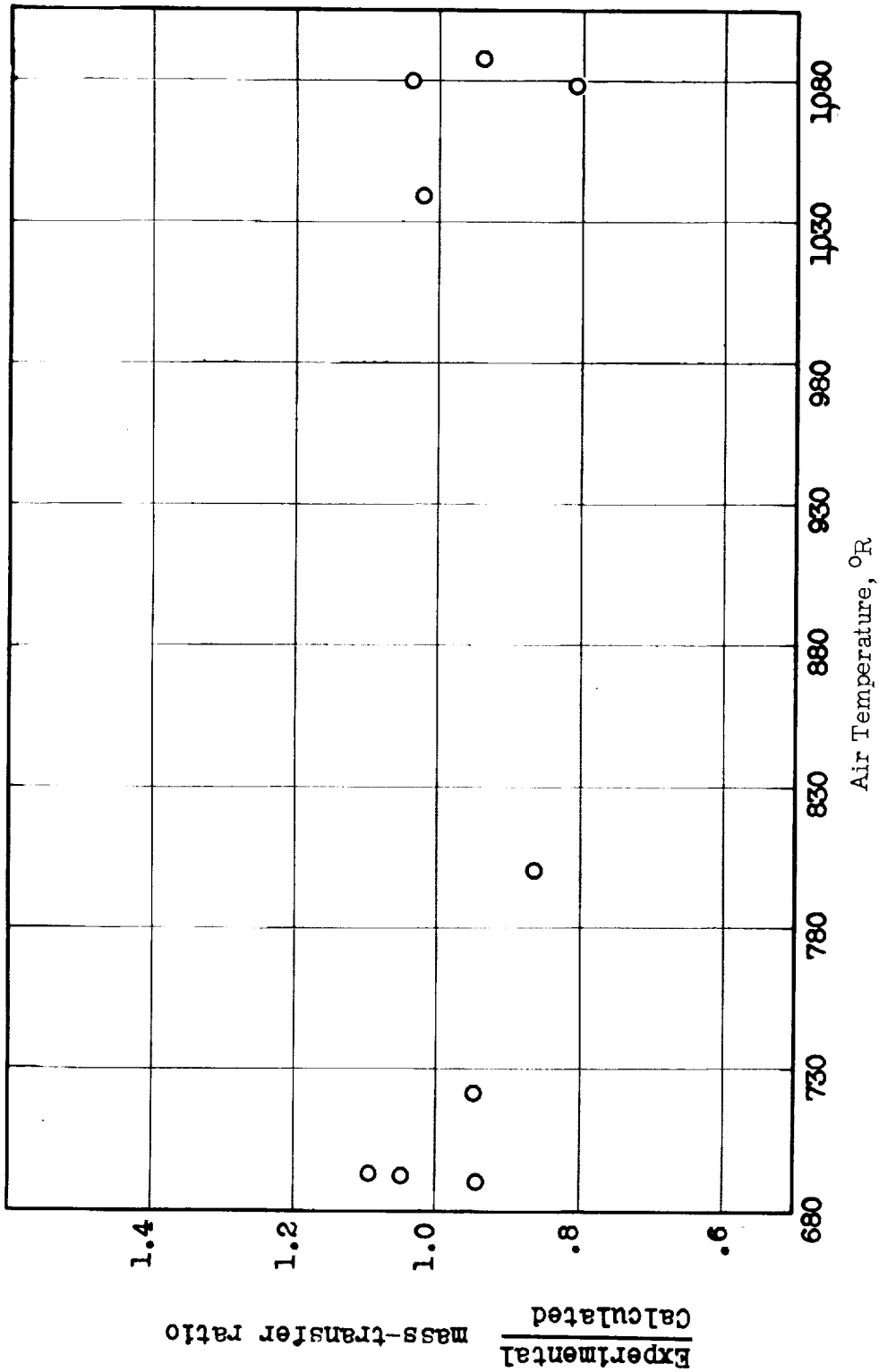

(a) Mass transfer during steady-state portion of temperature history.

Figure 22.- Ratio of experimental to calculated mass transfer.

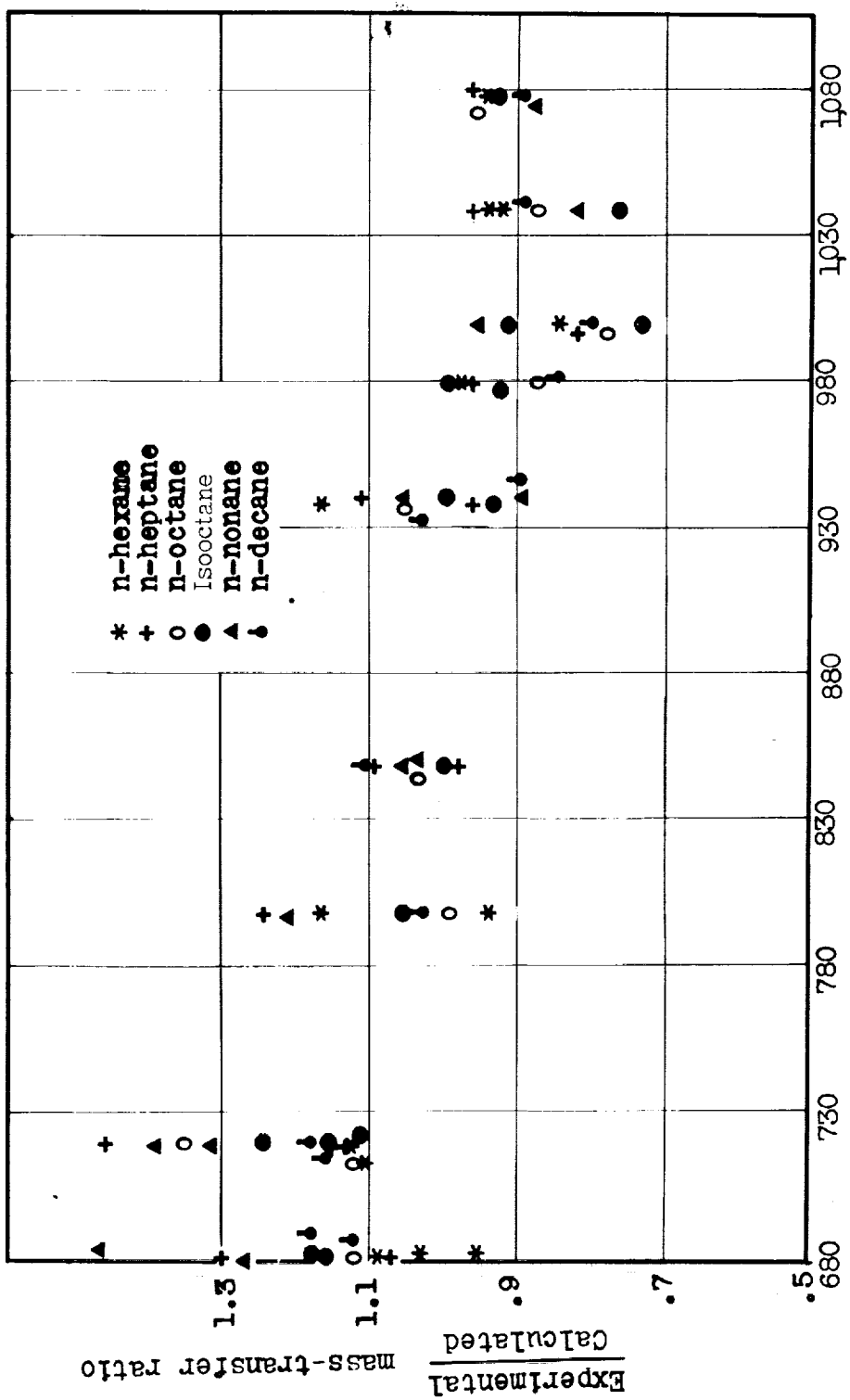

(b) Mass transfer calculated from experimental temperature histories for heating-up period.

Figure 22.- Concluded.

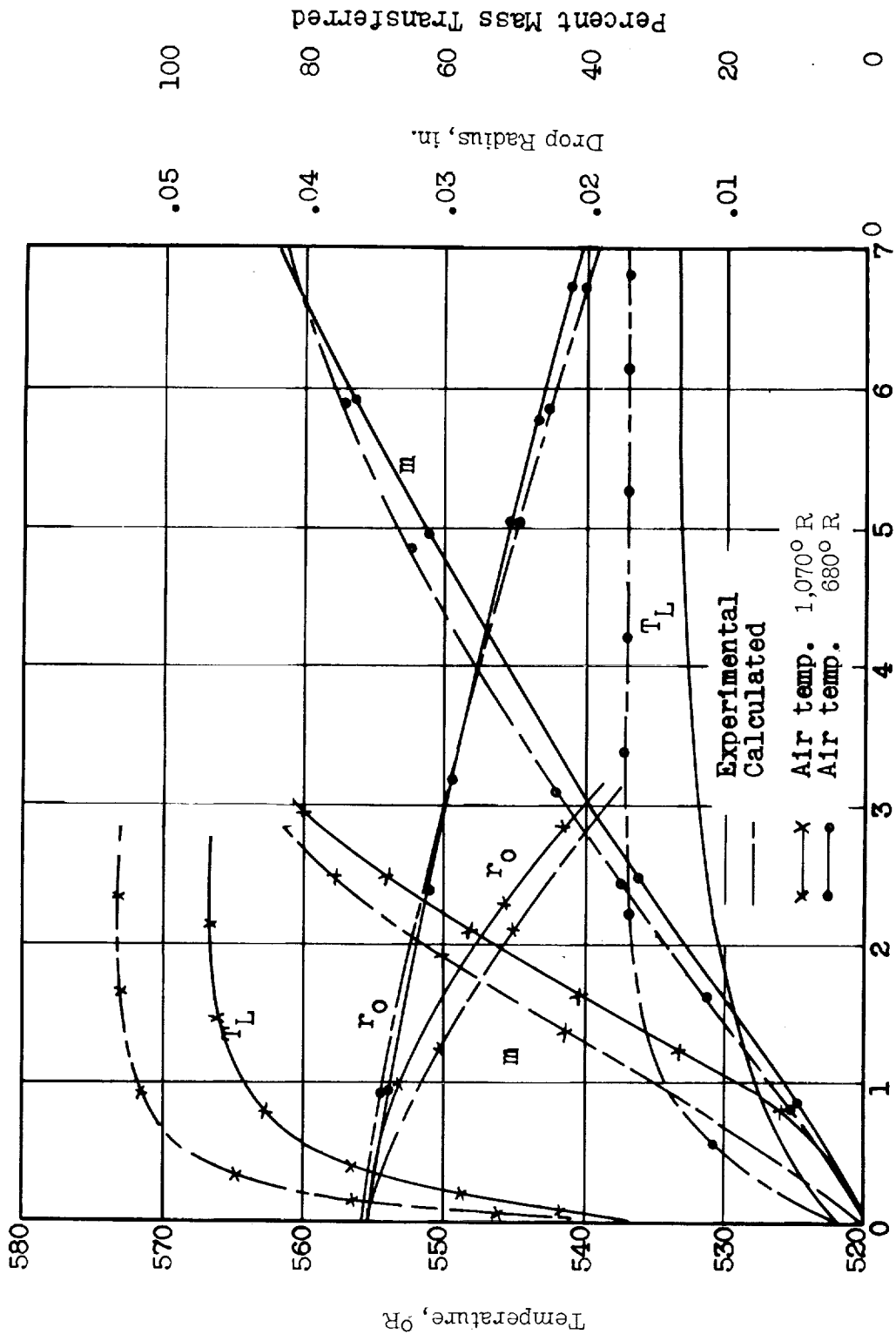

(a) n-Hexane.

Figure 23.- Experimental and calculated drop histories at different air temperatures. Air velocity, 90 inches per second.

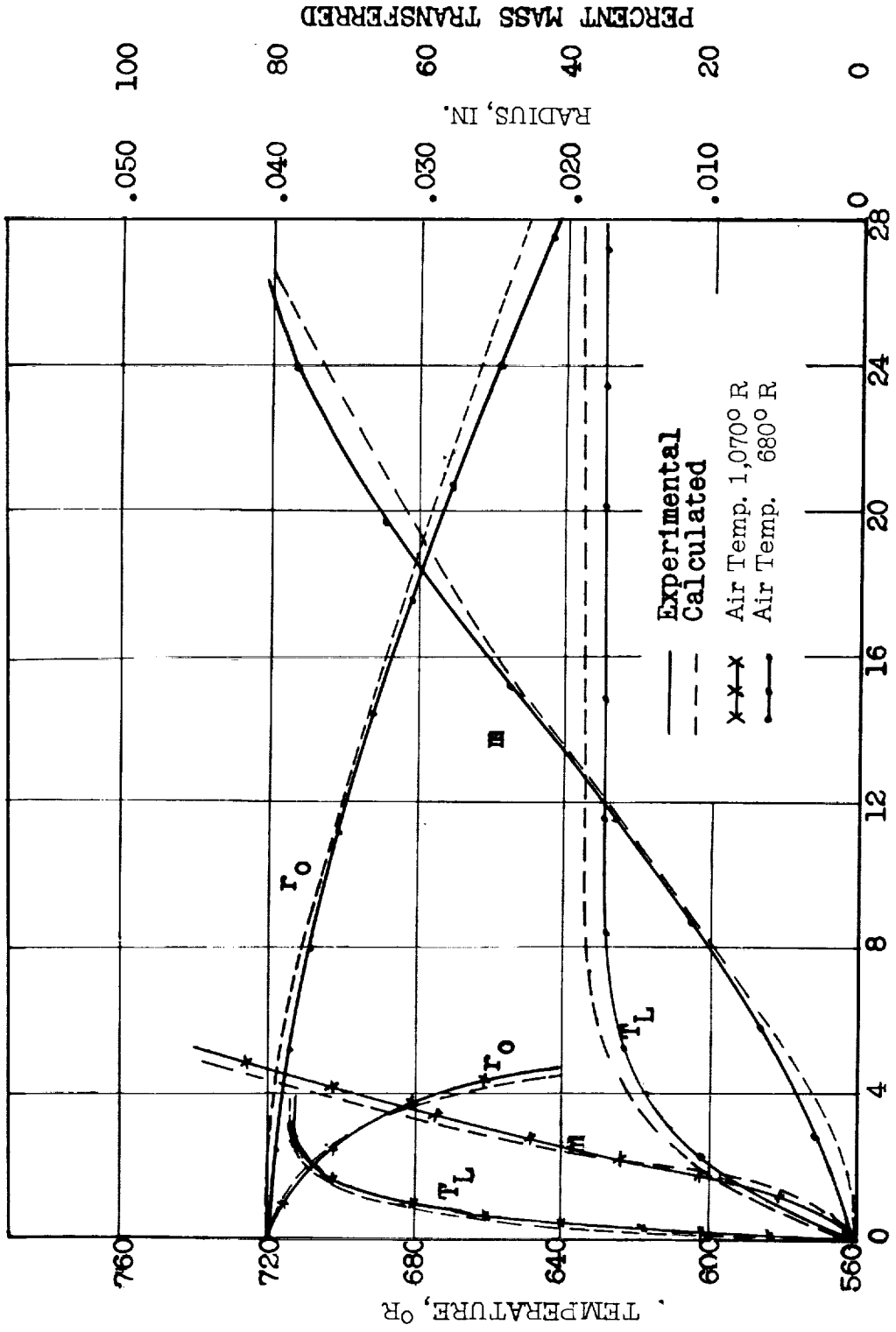

(b) n-Decane.

Figure 23.- Concluded.

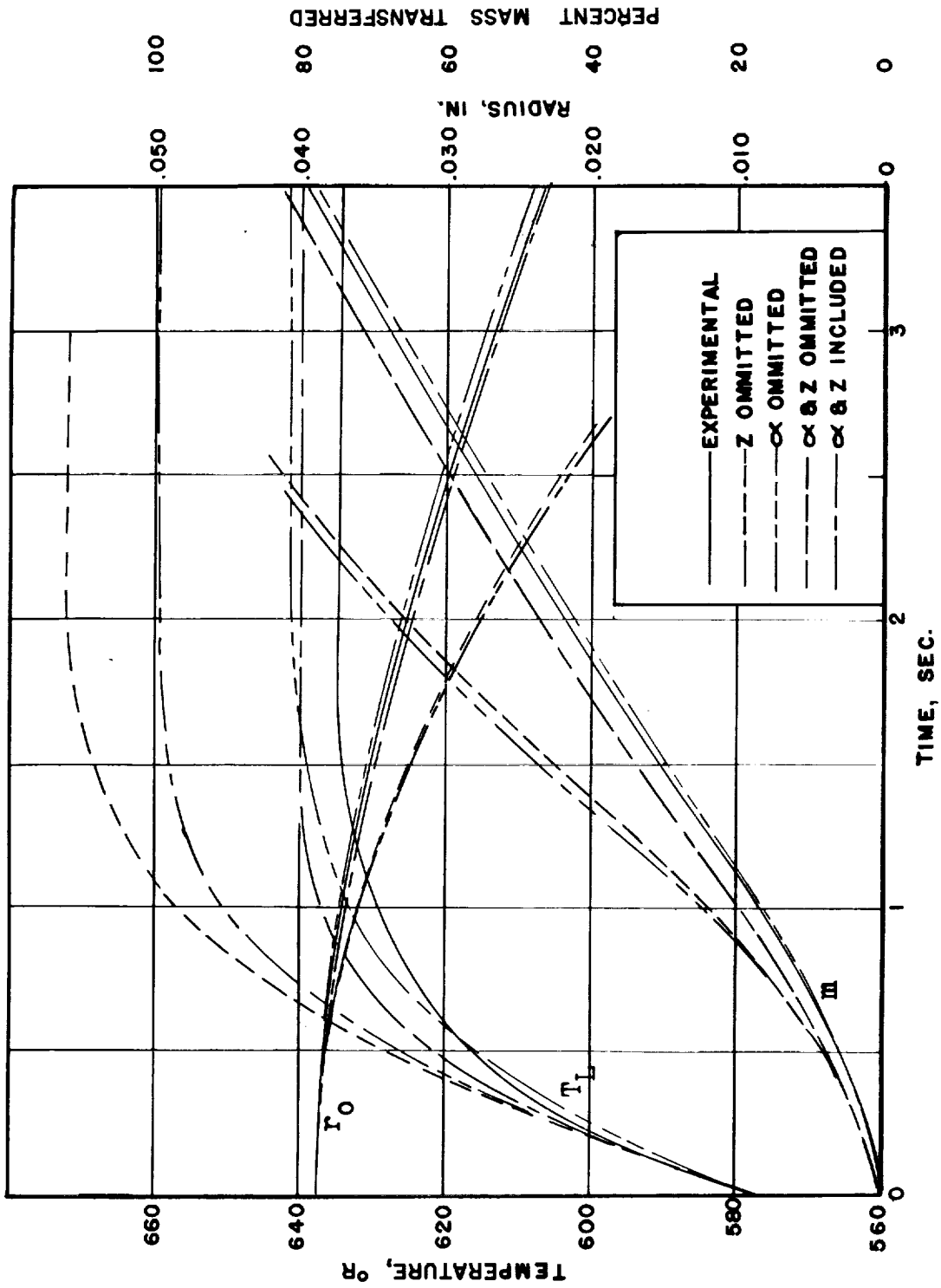

Figure 24.- Effect of α and Z factors on calculated histories.

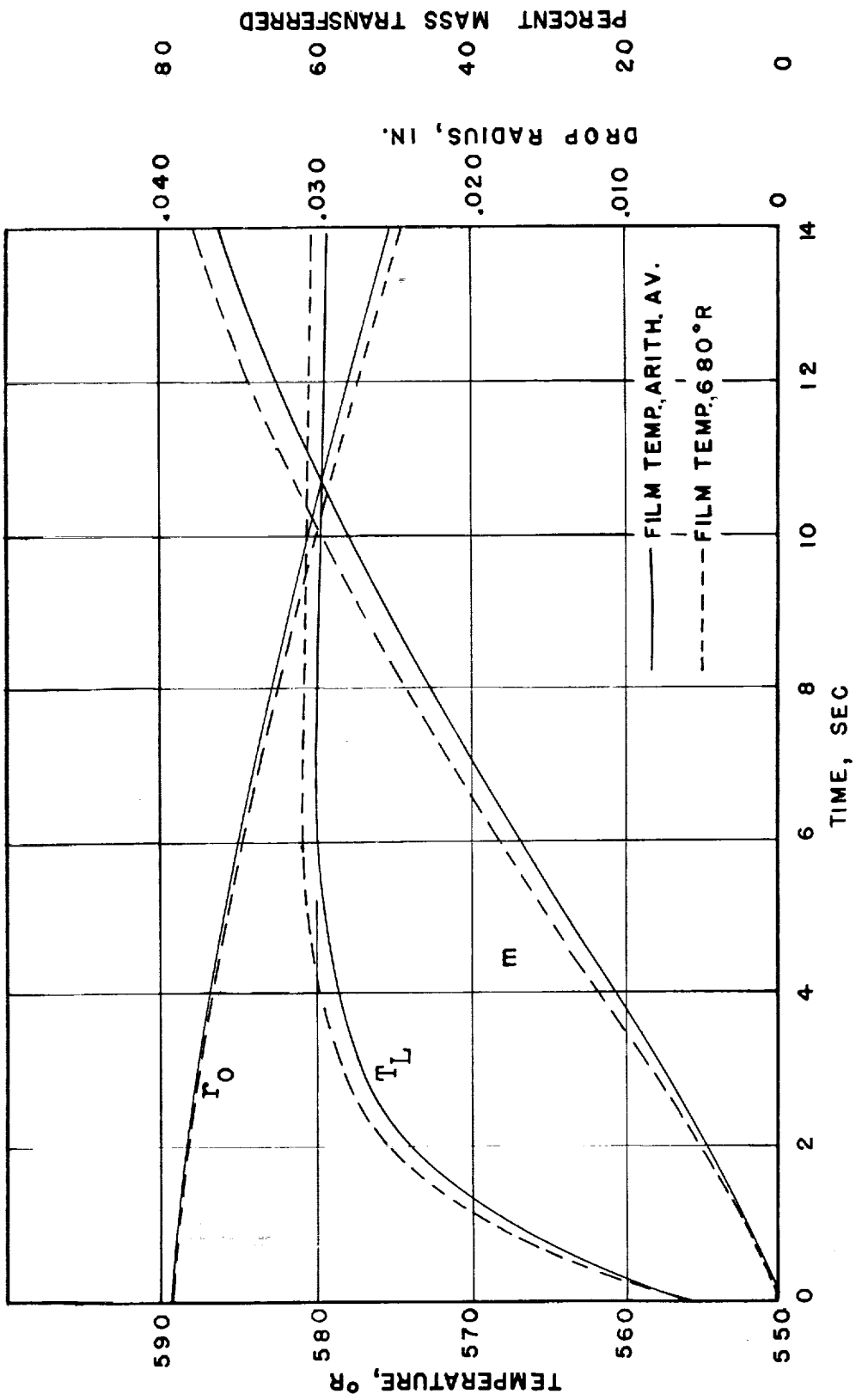

Figure 25.- Effect of film temperature averaging on physical properties. Fuel, n-octane; air temperature, 680° R.

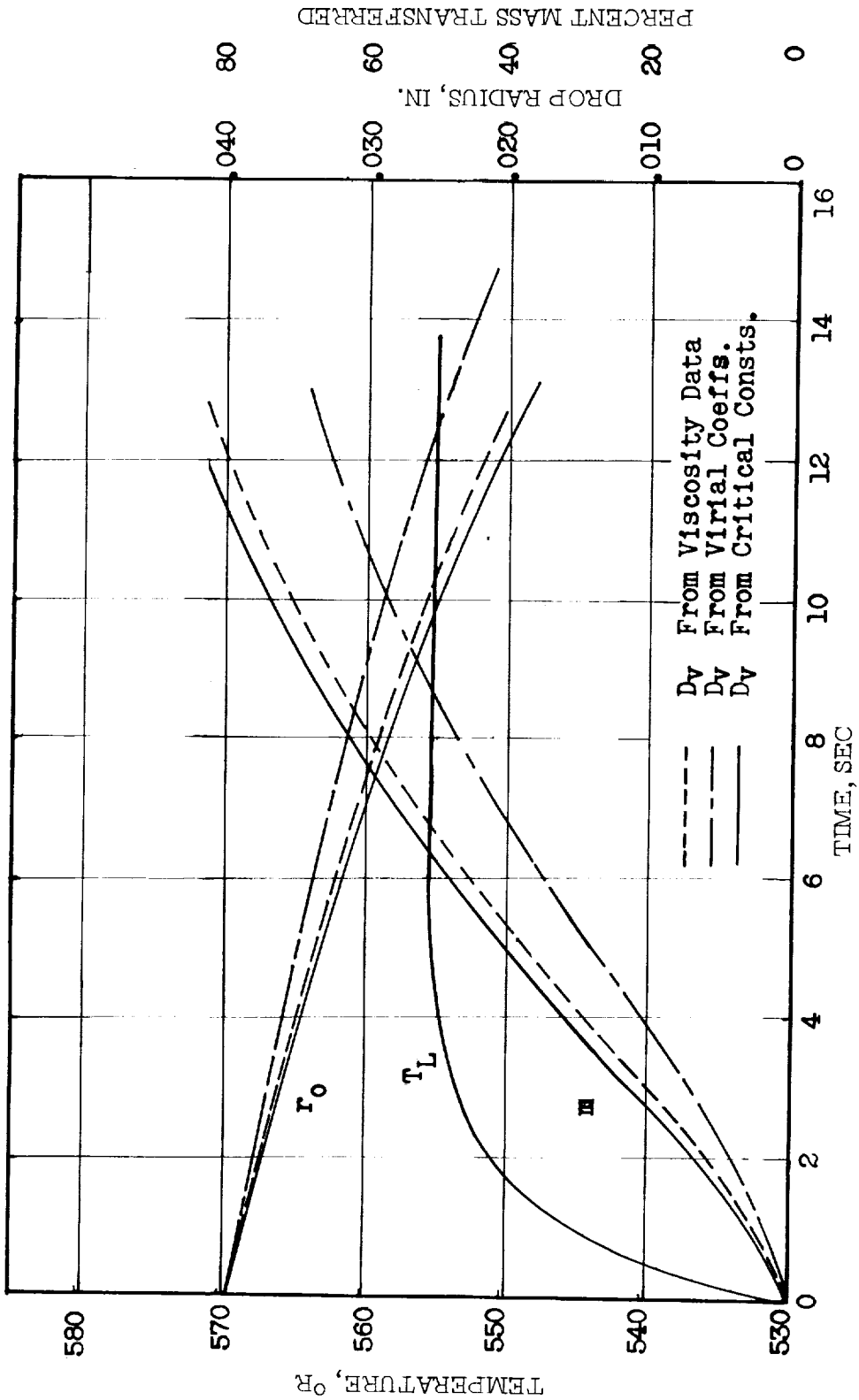

Figure 26.- Effect of different diffusion coefficients on calculated mass transfer. Fuel, n-heptane; air temperature, 676° R; air velocity, 84 inches per second.

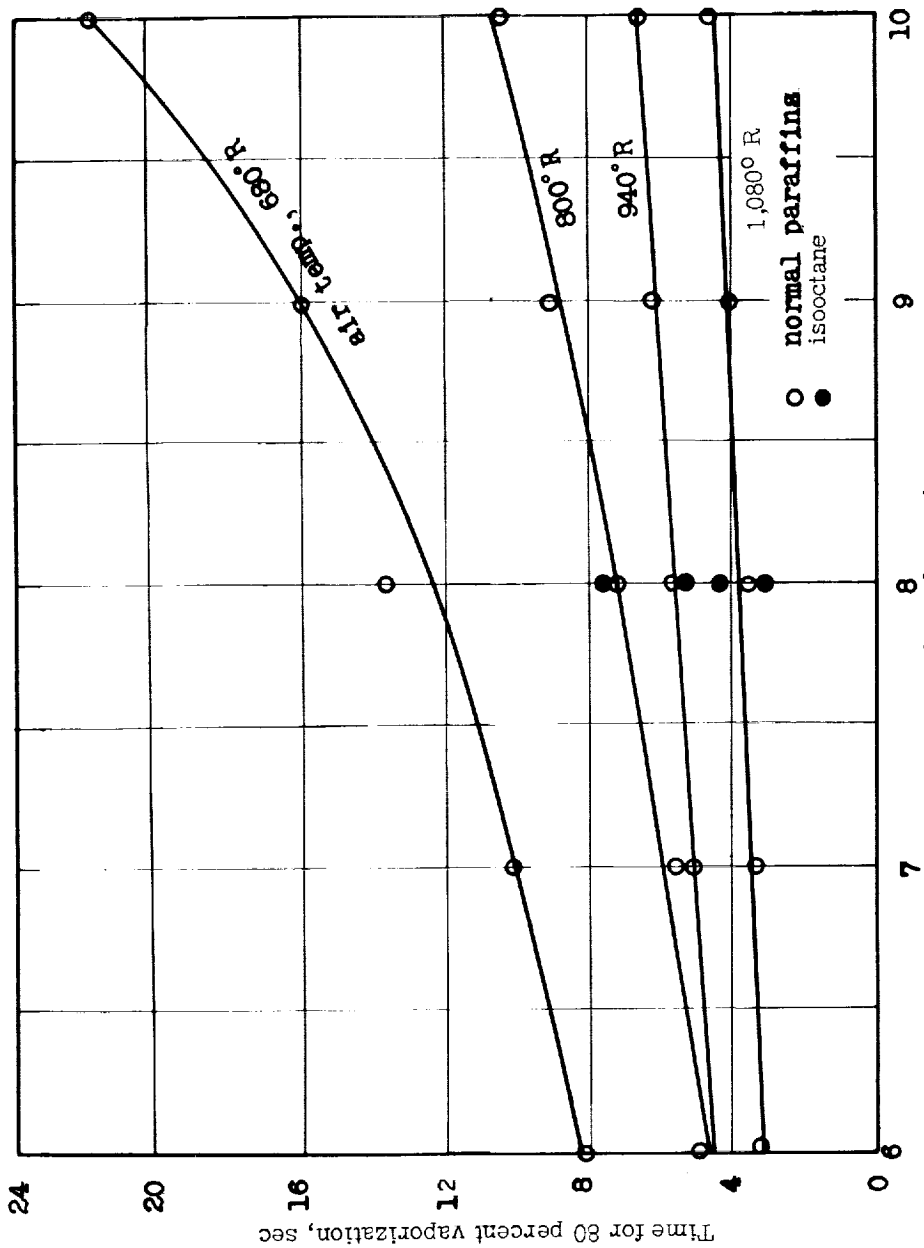

(a) Effect of fuel structure.

Figure 27.- Effect of fuel structure and air temperature on time for 80-percent vaporization of a drop. Initial radius, 0.039 inch; air velocity, 90 inches per second.

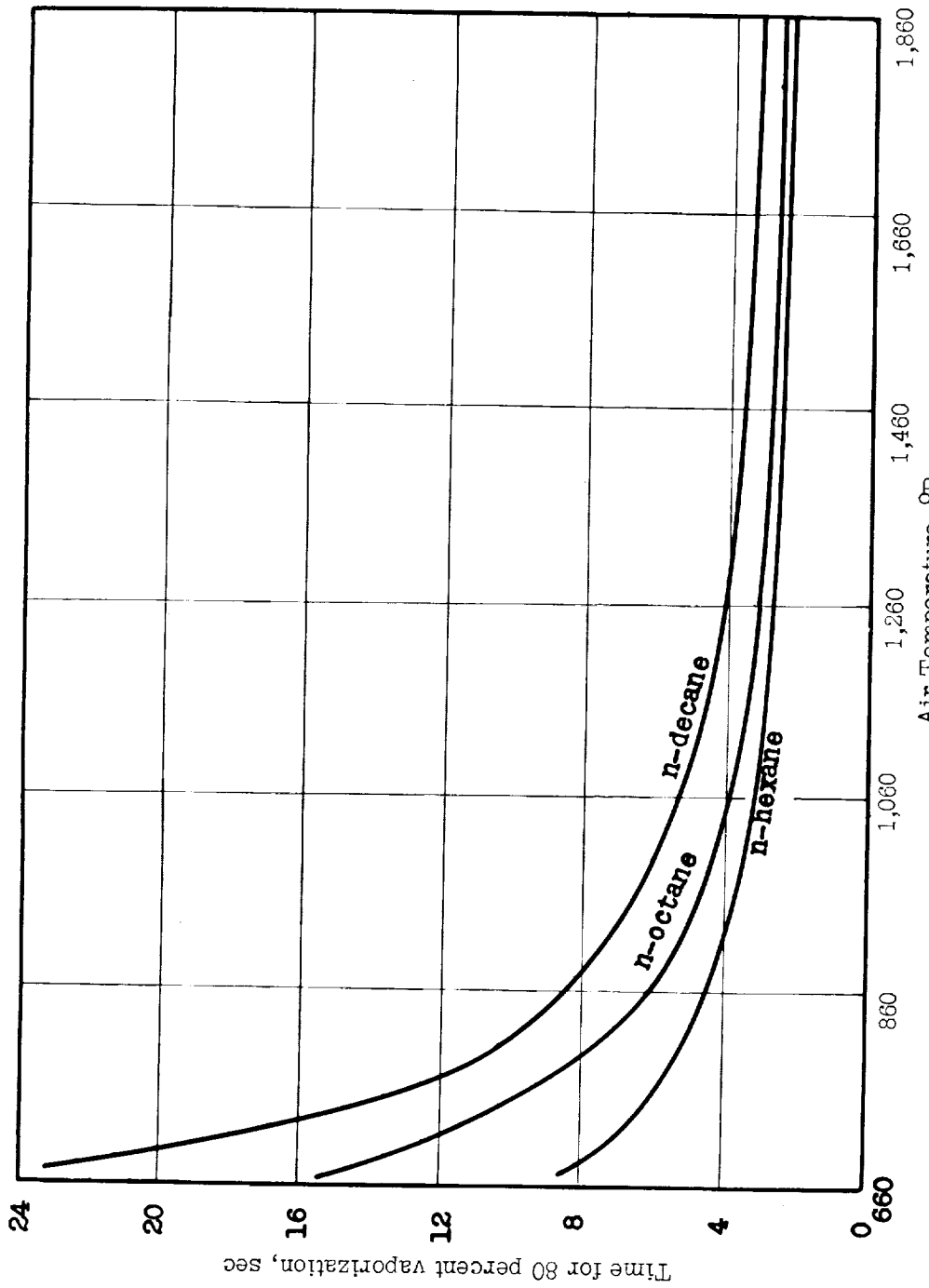

(b) Effect of air temperature.

Figure 27.- Concluded.

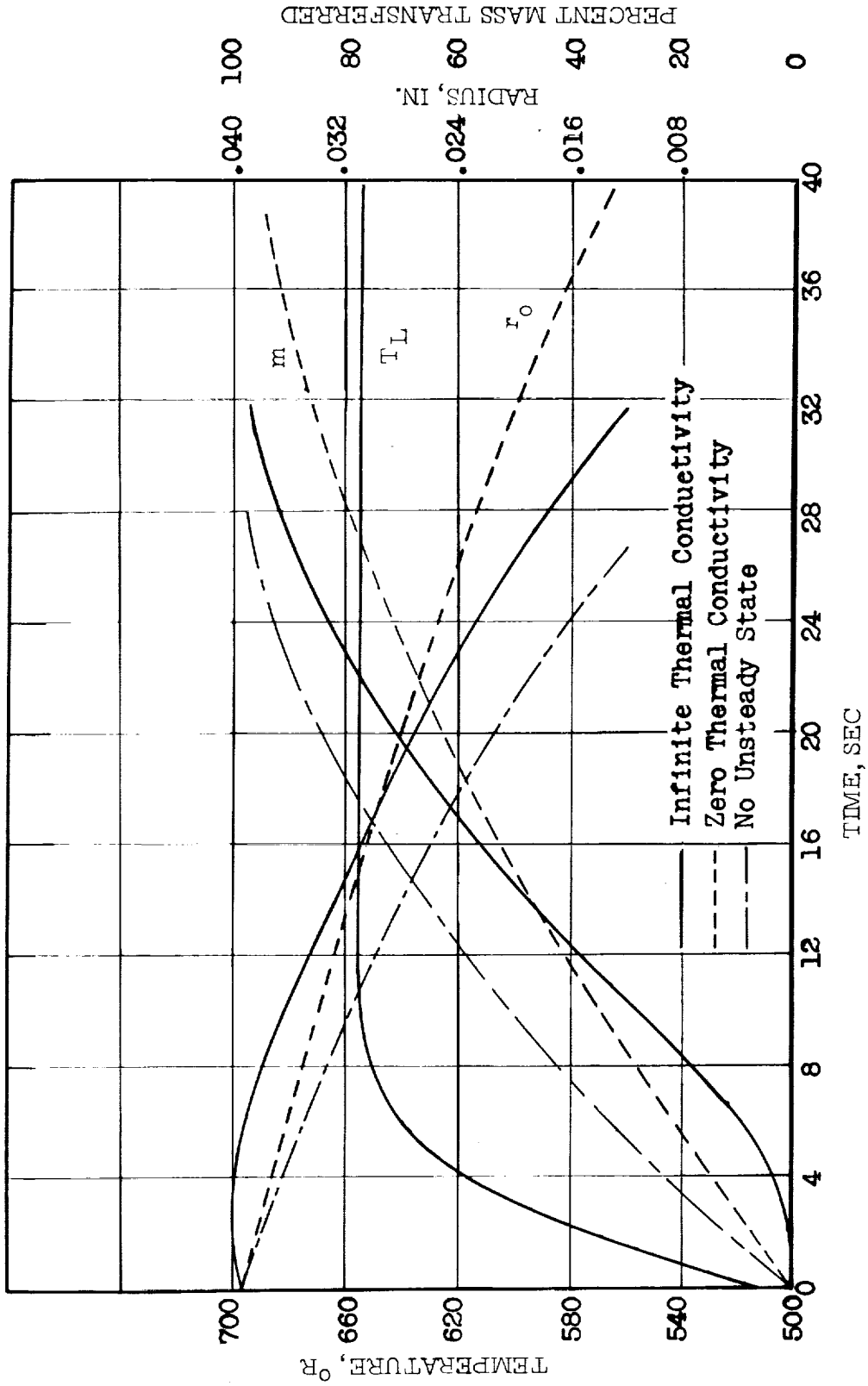

Figure 28.- Results of different calculation techniques. Fuel, n-octane; air temperature, 1,000° R; air velocity, 90 inches per second.